
AnyMo: Geometry-Aware Setup-Agnostic Modeling of Human Motion in the Wild

Baiyu Chen^{1*} Zechen Li¹ Wilson Wongso¹ Lihuan Li¹ Xiachong Lin¹
Hao Xue^{1,2,3} Benjamin Tag¹ Flora Salim^{1*}

¹The University of New South Wales

²The Hong Kong University of Science and Technology (Guangzhou)

³The Hong Kong University of Science and Technology

Abstract

As wearable and mobile devices become increasingly embedded in daily life, they offer a practical way to continuously sense human motion in the wild. But inertial signals are highly dependent on the sensing setup, including body location, mounting position, sensor orientation, device hardware, and sampling protocol. This setup dependence makes it difficult to learn motion representations that transfer across devices and datasets, and limits the broader use of wearable IMUs beyond closed-set recognition. We introduce AnyMo, a geometry-aware framework for setup-agnostic human motion modeling. AnyMo uses physics-grounded IMU simulation signals over dense body-surface placements to generate diverse and plausible synthetic signals, pre-trains a graph encoder from paired synthetic placement views and masked partial observations, tokenizes multi-position IMU into full-body motion tokens, and aligns these tokens with an LLM for motion-language understanding. We evaluate AnyMo on three complementary tasks: zero-shot activity recognition across 14 unseen downstream datasets, cross-modal retrieval, and wearable IMU motion captioning, where it improves average Accuracy/F1/R@2 by 11.7%/11.6%/22.6% on HAR, increases zero-shot IMU-to-text and text-to-IMU retrieval MRR by 15.9% and 28.6%, respectively, and improves zero-shot captioning BERT-F1 by 18.8%. These results support AnyMo as a generalist model for wearable motion understanding in the wild. Project page: <https://baiyuchen.com/project/AnyMo>.

1 Introduction

Human motion is one of the most immediate expressions of human context in everyday life [55, 1]. When people walk, cook, exercise, or interact with others or objects, their movement directly reflects their engagement with their surroundings over time. Understanding this context is important for future proactive AI and human-centered computing systems, which must proactively respond to changing user contexts and adapt in real environments rather than simply waiting for explicit commands [56, 12]. The growing ubiquity of wearable and mobile devices, from watches and phones to earbuds, smart rings, AR glasses, and body-worn sensors, creates new opportunities for sensing human motion in the wild, thus developing context-aware AI systems [7, 20, 8].

Yet sensing motion is not the same as understanding it. Inertial measurement unit (IMU) signals are semantically ambiguous: similar inertial patterns can arise from different activities depending on who is moving, how, and in what context. Resolving this ambiguity requires knowledge beyond closed-set activity labels. Language provides a natural source of such knowledge, as it is grounded in human descriptions of everyday behavior and supports compositional, open-ended semantics. Connecting

*Corresponding authors: breeze.chen@unsw.edu.au, flora.salim@unsw.edu.au.

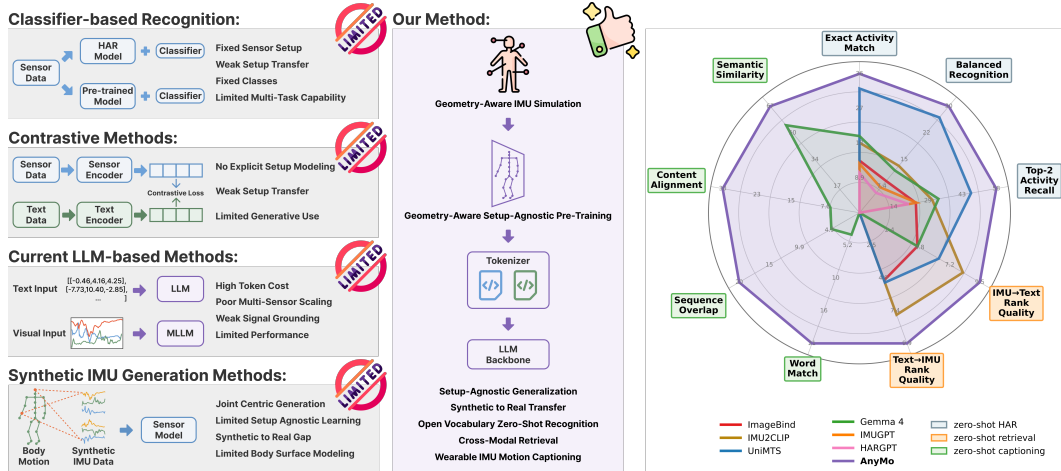


Figure 1: Method families for wearable human motion understanding and radar plot comparing the performance of AnyMo with baselines across various tasks and capabilities.

wearable sensing to language therefore helps models interpret motion in terms that generalize beyond fixed labels, making it central to generalist wearable motion understanding.

However, wearable IMU signals are tightly coupled to how and where the device is worn, making robust modeling difficult across sensing setups [8, 30, 9, 61]. A wrist-worn watch emphasizes arm motion, glasses capture head motion, and a phone in a pocket measures dynamics coupled to the torso and legs, even when the underlying activity is the same. Small changes in mounting position or orientation within a body part can further alter the measured acceleration and angular velocity, while device hardware and sampling introduce additional shifts [57, 24]. Consequently, models trained for one setup often struggle to transfer to another setup across users, devices, and datasets.

This setup dependence, combined with the challenges of grounding IMU in language, makes building a broadly useful wearable motion model difficult along three coupled axes [20, 8, 6]. ❶ **Data and Supervision Scarcity**: Real IMU data is difficult to collect at scale. It remains fragmented across body placements, device hardware, sampling rates, and datasets, and supervision is often limited to a small closed set of coarse activity labels rather than rich descriptions of how motion unfolds. ❷ **Limited Realism of Synthetic Augmentation**: Synthetic or augmented sensor data must expand setup coverage without losing physical realism, but existing generation pipelines often remain tied to specific labels, activities, or sparse sensor placements. ❸ **Modality Gap**: Connecting IMU to language requires bridging continuous, multi-sensor motion signals with discrete textual concepts, a modality gap that direct prompting or simple contrastive alignment does not fully resolve and that grows more severe as the number of sensors, channels, and body locations increases. Figure 1 contextualizes these issues across classifier-based, contrastive, LLM-based, and synthetic-generation methods, which address parts of the problem but remain limited along different axes.

These challenges motivate our key insight: **wearable setup variation is structured rather than arbitrary**. An IMU is attached to a body surface, and its signal is produced by the interaction of body motion, surface geometry, sensor orientation, and device response. This structure provides a geometry- and physics-based inductive bias for learning setup-robust body motion representations. We further argue that **language should be connected to wearable sensing through a compact motion representation rather than raw IMU streams**. Language models provide priors for open-vocabulary motion understanding, but raw numerical IMU tokens scale with sensors, channels, and time, while sensor location-specific tokenizers tie representations to fixed setups. Compact full-body tokens avoid both limitations, providing a stable interface between motion and language.

With these insights, we introduce **AnyMo**, a geometry-aware framework for setup-agnostic human motion modeling in the wild. It aims to learn robust IMU representations across **Any** wearable setup for human **Motion** understanding. As shown in Figure 1, AnyMo connects **physics-grounded geometry-aware IMU simulation** with **geometry-aware setup-agnostic pre-training**, **full-body tokenization**, and **motion-language alignment**. The simulation stage generates dense geometry-

aware IMU candidates over body-surface placements, providing a broad and plausible distribution of wearable locations and orientations. The pre-training stage constructs paired placement views and masked wearable observations, encouraging the encoder to learn setup-agnostic motion representations. The tokenizer converts multi-position IMU observations into compact full-body motion tokens, aligned with an LLM for open-vocabulary recognition, cross-modal retrieval, and motion captioning.

To validate AnyMo, we benchmark it against state-of-the-art methods on three complementary tasks: zero-shot activity recognition, unseen cross-modal retrieval, and wearable IMU motion captioning. For zero-shot recognition, we use 14 completely unseen downstream datasets spanning classic HAR benchmarks and in-the-wild settings. Retrieval and captioning are evaluated under sim-to-real transfer on unseen Nymeria subjects and out-of-domain (OOD) zero-shot transfer to EgoExo4D. Across all tasks, AnyMo shows significant gains over baselines, establishing it as a generalist model for wearable motion understanding. Our contributions are as follows:

❶ **We propose physics-grounded, geometry-aware IMU simulation** over dense body-surface placements, providing diverse and plausible synthetic signals that bridge synthetic pre-training and real wearable IMU. ❷ **We develop a setup-agnostic representation learning method and full-body IMU tokenization**, aligning motion across synthetic placement views and mapping multi-position IMU into full-body motion tokens. ❸ **We introduce an IMU-language generalist model** that supports a variety of wearable motion understanding tasks.

2 Related Works

Wearable Motion Representations and Setup Transfer. Recent wearable motion models improve generalization through synthetic pretraining [78, 33, 32, 43, 67], large-scale self-supervision or cross-dataset adaptation [70, 24], and tokenization [76]. Other works study setup variation via cross-location transfer [14], simulated body-surface placement analysis [52], or coordinate-conditioned flexible placement [83]; however, they remain mainly recognition- or pose-centered and do not combine dense local surface-frame simulation, setup-agnostic pretraining, full-body tokenization, and motion-language generation. **Sensor-Language and Cross-Modal Grounding.** Sensor-language and multimodal methods connect IMU or broader human-sensing signals to language, LLM reasoning, shared embedding spaces, or cross-modal supervision [80, 39, 36, 27, 4, 65, 59, 44, 16, 82, 32, 33, 10, 63, 35, 23, 66, 28, 46, 29]. Embedding and instruction-tuning methods [75, 31, 45] further motivate joint retrieval and generation training, but these works do not directly address sparse, setup-dependent wearable IMU through geometry-aware full-body tokenization. **Self-Supervised Skeleton and Graph Motion Pretraining.** Skeleton and graph self-supervised methods [71, 41, 26, 37, 25, 34] motivate our use of masked motion modeling, graph encoders, and cross-view consistency, but these works focus on pose or skeleton observations rather than sparse wearable inertial signals.

3 Methodology

Building on the observation that wearable setup variation is structured, AnyMo targets wearable IMU motion understanding under variable sensing setups. We follow the Nymeria [40] body model and organize motion over $N_{\text{seg}} = 23$ anatomical segments. We denote an IMU window as $\mathbf{x} \in \mathbb{R}^{T \times 6}$, where the last dimension contains three-axis acceleration and three-axis angular velocity. The same motion can therefore yield different IMU windows across different wearable setups, whereas a real device typically provides only a partial observation of the body. AnyMo aims to learn a representation that absorbs such partial, setup-specific IMU windows and preserves motion information that is useful across sensing setups and language-based tasks. Figure 1 illustrates the proposed pipeline with three key enablers: geometry-aware IMU simulation (Section 3.1), setup-agnostic representation learning (Section 3.2), and full-body IMU tokenization with motion-language alignment (Section 3.3).

3.1 Physics-Grounded Geometry-Aware Motion Simulation

Motion skeleton and mesh data describe human body motion through segment positions, orientations, and posed body-surface geometry over time [40]. Wearable IMUs, however, measure local acceleration and angular velocity rather than body pose directly. We synthesize wearable IMU windows by applying wearable IMU motion equations [47] to synchronized Nymeria body motion. Unlike joint-centric simulation [78, 32, 33, 67, 43], our goal is to model plausible wearable locations on the

body surface, together with their local sensor frames and device noise. For each anatomical segment i , let \mathcal{V}_i denote the selected candidate surface vertices on the Nymeria template body mesh. We compute a segment centroid \mathbf{c}_i as the weighted average of the selected template vertices in \mathcal{V}_i .

To define a consistent in-surface direction, we set an anatomical axis \mathbf{u}_i from \mathbf{c}_i toward the centroid of its nearest available child segment in the body kinematic tree, or along the opposite direction from its nearest available parent when no child segment is available. For each vertex $v \in \mathcal{V}_i$, we compute a surface normal $\mathbf{n}_{i,v}$ from the template mesh faces. The normal defines a local tangent plane. We choose the tangent direction $\mathbf{t}_{i,v}$ by projecting \mathbf{u}_i onto this plane, set the binormal $\mathbf{b}_{i,v} = \mathbf{n}_{i,v} \times \mathbf{t}_{i,v}$, and form a right-handed surface-based sensor frame $\mathbf{R}_{i,v}^{\text{surf}} = [\mathbf{t}_{i,v}, \mathbf{b}_{i,v}, \mathbf{n}_{i,v}]$:

$$\mathbf{t}_{i,v} = (\mathbf{u}_i - (\mathbf{u}_i^\top \mathbf{n}_{i,v}) \mathbf{n}_{i,v}) / \|\mathbf{u}_i - (\mathbf{u}_i^\top \mathbf{n}_{i,v}) \mathbf{n}_{i,v}\|_2. \quad (1)$$

Let $\mathbf{p}_i(t)$, $\mathbf{R}_i(t)$, and $\mathbf{m}_v(t)$ denote the global segment position, global segment orientation, and posed mesh vertex position. We estimate the local virtual sensor offset by $\mathbf{r}_{i,v} = \frac{1}{T} \sum_{t=1}^T \mathbf{R}_i(t)^\top (\mathbf{m}_v(t) - \mathbf{p}_i(t))$. To account for mounting orientation variation during synthesis, we sample an in-plane rotation $\Delta \mathbf{R}_{i,v}$ around the surface normal and obtain the final local sensor frame $\tilde{\mathbf{R}}_{i,v}^{\text{surf}} = \Delta \mathbf{R}_{i,v} \mathbf{R}_{i,v}^{\text{surf}}$. The virtual IMU trajectory is then defined by its global position $\mathbf{p}_{i,v}^{\text{imu}}(t) = \mathbf{p}_i(t) + \mathbf{R}_i(t) \mathbf{r}_{i,v}$ and orientation $\mathbf{R}_{i,v}^{\text{imu}}(t) = \mathbf{R}_i(t) \tilde{\mathbf{R}}_{i,v}^{\text{surf}}$. The accelerometer $\mathbf{a}_{i,v}(t)$ is obtained by transforming the second-order derivative of the virtual sensor position into the local sensor frame and removing gravity, while the gyroscope $\boldsymbol{\omega}_{i,v}(t)$ is computed from the temporal change of the virtual sensor orientation:

$$\begin{aligned} \mathbf{a}_{i,v}(t) &= \mathbf{R}_{i,v}^{\text{imu}}(t)^\top (d^2 \mathbf{p}_{i,v}^{\text{imu}}(t) / dt^2 - \mathbf{g}) + \boldsymbol{\eta}_{i,v}^a(t), \\ \boldsymbol{\omega}_{i,v}(t) &= \mathbf{R}_{i,v}^{\text{imu}}(t)^\top \Omega(\mathbf{R}_{i,v}^{\text{imu}}(t)) + \boldsymbol{\eta}_{i,v}^\omega(t). \end{aligned} \quad (2)$$

Here \mathbf{g} denotes gravity, $\Omega(\cdot)$ maps an orientation trajectory to angular velocity, and $\boldsymbol{\eta}_{i,v}^a(t)$ and $\boldsymbol{\eta}_{i,v}^\omega(t)$ denote accelerometer and gyroscope noise. To reflect real device variability, we estimate two hardware-style noise priors from quiet windows of two real Nymeria IMU streams and randomly assign these priors to synthetic placements. The final synthetic IMU candidate for placement (i, v) is $\mathbf{x}_{i,v}(t) = [a_{i,v}^x(t), a_{i,v}^y(t), a_{i,v}^z(t), \omega_{i,v}^x(t), \omega_{i,v}^y(t), \omega_{i,v}^z(t)]$. Collecting $\mathbf{x}_{i,v}$ over all selected vertices and anatomical segments yields a dense, geometry-aware distribution of wearable setups for pre-training. We evaluate the contribution of this geometry-aware simulation design in Table 4.

3.2 Geometry-Aware Setup-Agnostic Pre-Training

The dense simulation in Section 3.1 provides multiple plausible IMU candidates for the same body motion, but downstream wearable inputs are sparse and setup-specific. Even within the same body segment, different surface placements and sensor orientations can produce different IMU windows. These setup variations are nevertheless organized by a fixed body topology: each synthetic IMU candidate is associated with one Nymeria anatomical segment, and segment motions are coupled through the body kinematic tree. We use this structure to represent a full-body IMU observation as a spatio-temporal graph, where node i stores the IMU window sampled for segment i and edges follow the Nymeria kinematic tree. Following spatial-temporal graph convolutional networks [72], the graph encoder models temporal dynamics and cross-segment motion correlations while treating surface placement and mounting orientation as within-segment setup variation. This requires a representation that remains stable across synthetic setup changes while retaining temporal motion structure beyond coarse activity labels. As shown in Figure 3, we sample paired synthetic placement views from these candidates to train a setup-agnostic graph encoder and a full-body IMU tokenizer.

Masked Cross-View Predictive Contrastive Learning. A natural choice is to contrast the two full graph views, following graph and skeleton contrastive representation learning [26, 37, 34]. However, full-view graph contrast can be satisfied by aligning complete body observations, so it does not

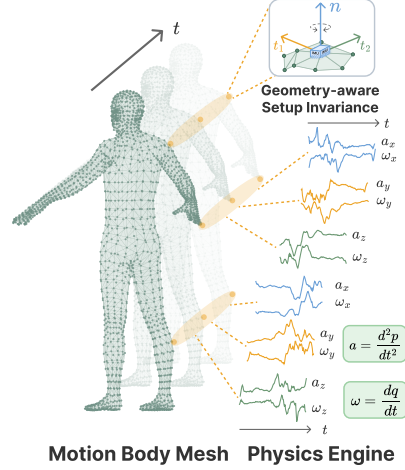


Figure 2: Physics-grounded geometry-aware motion simulation.

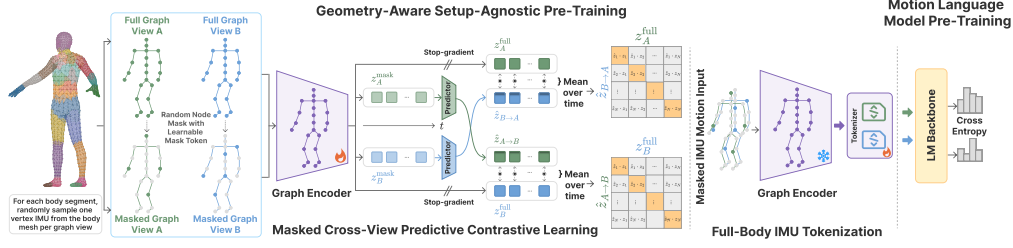


Figure 3: Details of (1) Geometry-Aware Pre-Training, (2) Full-Body IMU Tokenization and (3) Motion Language Model Pre-Training.

teach the encoder to infer full-body motion from sparse wearable inputs. Masked modeling methods address sparsity by reconstructing masked graph or motion tokens [71, 41, 25], but masked prediction alone does not explicitly separate different motion instances. Moreover, collapsing a motion window into a single clip-level embedding would remove the temporal structure needed by the tokenizer. We therefore design a masked cross-view predictive contrastive objective that combines sparse-to-full recovery, contrastive discrimination, and time-preserving sequence latents. Concretely, we predict the full-view latent of one synthetic setup from the masked observation of another setup, and contrast the prediction against other motion windows in the batch. We further analyze the importance of this learning objective through ablation and embedding visualization in Table 4 and Figure 6.

As illustrated in Figure 3, for each motion window we construct two full graph views A and B by independently sampling candidate placements $v_i^A, v_i^B \in \mathcal{V}_i$ for every segment i . For each selected placement, we sample one local mounting rotation $\Delta \mathbf{R}_i^A$ or $\Delta \mathbf{R}_i^B$. The rotation combines in-plane rotation around the surface normal with a small tilt around the local tangent axes to approximate imperfect surface attachment. For an IMU candidate $\mathbf{x}_{i,v}(t) = [\mathbf{a}_{i,v}(t); \boldsymbol{\omega}_{i,v}(t)]$, rotation augmentation applies the same local rotation to acceleration and angular velocity, yielding paired full graph views $\mathbf{X}^A, \mathbf{X}^B \in \mathbb{R}^{T \times N_{\text{seg}} \times 6}$, where $\mathbf{X}_{t,i}^A := [\Delta \mathbf{R}_i^A \mathbf{a}_{i,v_i^A}(t); \Delta \mathbf{R}_i^A \boldsymbol{\omega}_{i,v_i^A}(t)]$ and $\mathbf{X}_{t,i}^B := [\Delta \mathbf{R}_i^B \mathbf{a}_{i,v_i^B}(t); \Delta \mathbf{R}_i^B \boldsymbol{\omega}_{i,v_i^B}(t)]$. We then create masked graph views by randomly keeping between one and five visible segment nodes and replacing all other segment nodes with a learnable mask token, as shown in Figure 3. Let \mathcal{M}^A and \mathcal{M}^B denote the visible segment sets. The shared spatio-temporal graph encoder \mathcal{G}_θ produces node-level sequence features and averages over segment nodes to obtain time-preserving latents in $\mathbb{R}^{T' \times d}$, where T' is the encoder output length and d is the latent dimension. We write the full-view latents as $\mathbf{z}_A^{\text{full}} = \mathcal{G}_\theta(\mathbf{X}^A)$ and $\mathbf{z}_B^{\text{full}} = \mathcal{G}_\theta(\mathbf{X}^B)$, and the masked-view latents as $\mathbf{z}_A^{\text{mask}} = \mathcal{G}_\theta(\text{Mask}(\mathbf{X}^A, \mathcal{M}^A))$ and $\mathbf{z}_B^{\text{mask}} = \mathcal{G}_\theta(\text{Mask}(\mathbf{X}^B, \mathcal{M}^B))$. A temporal predictor q_ϕ , implemented as a six-layer Transformer [64], predicts the opposite full-view latent: $\hat{\mathbf{z}}_{A \rightarrow B} = q_\phi(\mathbf{z}_A^{\text{mask}})$ and $\hat{\mathbf{z}}_{B \rightarrow A} = q_\phi(\mathbf{z}_B^{\text{mask}})$.

We train the encoder and predictor with a cross-view predictive InfoNCE loss, using mean cosine similarity over time for predicted and target sequence latents $\hat{\mathbf{z}}, \mathbf{z} \in \mathbb{R}^{T' \times d}$, defined as $s(\hat{\mathbf{z}}, \mathbf{z}) = \frac{1}{T'} \sum_{\ell=1}^{T'} \frac{\hat{\mathbf{z}}_\ell^\top \mathbf{z}_\ell}{\|\hat{\mathbf{z}}_\ell\|_2 \|\mathbf{z}_\ell\|_2}$. For a minibatch of N_{batch} windows, the $A \rightarrow B$ loss is:

$$\mathcal{L}_{A \rightarrow B} = -\frac{1}{N_{\text{batch}}} \sum_{n=1}^{N_{\text{batch}}} \log \frac{\exp(s(\hat{\mathbf{z}}_{A \rightarrow B}^{(n)}, \text{sg}(\mathbf{z}_B^{\text{full},(n)})) / \tau)}{\sum_{m=1}^{N_{\text{batch}}} \exp(s(\hat{\mathbf{z}}_{A \rightarrow B}^{(n)}, \text{sg}(\mathbf{z}_B^{\text{full},(m)})) / \tau)}. \quad (3)$$

The $B \rightarrow A$ loss is defined symmetrically, and the final objective is $\mathcal{L}_{\text{MCVPCL}} = \mathcal{L}_{A \rightarrow B} + \mathcal{L}_{B \rightarrow A}$. Here $\text{sg}(\cdot)$ denotes stop-gradient and τ is temperature, (n) and (m) index windows in the minibatch.

Full-Body IMU Tokenization. Pre-training produces continuous, setup-stable sequence latents, while the motion-language model requires compact discrete inputs. As motivated in Section 1, feeding raw IMU streams into an LLM is inefficient. To connect wearable motion with language models, we train a full-body IMU tokenizer that discretizes the frozen graph encoder latent into compact IMU tokens, following recent motion-language tokenizers based on product quantization [23].

As shown in Figure 3, with additional details in Figure 7, we freeze \mathcal{G}_θ and train a product-quantized VAE tokenizer on the latent obtained from masked wearable observations $\mathbf{z}^{\text{mask}} = \mathcal{G}_\theta(\text{Mask}(\mathbf{X}, \mathcal{M})) \in \mathbb{R}^{T' \times d}$. A projection maps each timestep latent $\mathbf{z}_\ell^{\text{mask}}$ to a lower-dimensional projected latent $\bar{\mathbf{z}}_\ell \in \mathbb{R}^{\bar{d}}$. Let P denote the number of product codebooks and K denote the num-

ber of entries in each codebook. We evenly split $\bar{\mathbf{z}}_\ell$ into P chunks $\{\bar{\mathbf{z}}_{\ell,j} \in \mathbb{R}^{\bar{d}/P}\}_{j=1}^P$, where j indexes the product subspace. The j -th codebook is $\mathcal{E}_j = \{\mathbf{e}_{j,k} \in \mathbb{R}^{\bar{d}/P}\}_{k=1}^K$, where $\mathbf{e}_{j,k}$ is the k -th code vector in that codebook. Each chunk is quantized to its nearest code vector: $\kappa_{\ell,j} = \arg \min_{k \in \{1, \dots, K\}} \|\bar{\mathbf{z}}_{\ell,j} - \mathbf{e}_{j,k}\|_2^2$, and the concatenated quantized latent $\mathbf{q}_\ell = [\mathbf{e}_{1,\kappa_{\ell,1}}; \dots; \mathbf{e}_{P,\kappa_{\ell,P}}]$, where $\kappa_{\ell,j}$ is the discrete code index for timestep ℓ and product subspace j , and \mathbf{q}_ℓ is the concatenated quantized latent. A temporal convolutional decoder takes quantized sequence $\mathbf{q} = [\mathbf{q}_1, \dots, \mathbf{q}_{T'}]$ and reconstructs $\tilde{\mathbf{z}} = D(\mathbf{q})$. We optimize the tokenizer with a reconstruction and commitment objective:

$$\mathcal{L}_{\text{com}} = \sum_{j=1}^P \frac{P}{T'd} \sum_{\ell=1}^{T'} \|\bar{\mathbf{z}}_{\ell,j} - \text{sg}(\mathbf{e}_{j,\kappa_{\ell,j}})\|_2^2, \quad \mathcal{L}_{\text{tok}} = \text{SmoothL1}(\tilde{\mathbf{z}}, \mathbf{z}^{\text{mask}}) + \lambda_{\text{com}} \mathcal{L}_{\text{com}}. \quad (4)$$

We update codebooks with exponential moving averages and refresh dead codes to maintain codebook usage. Finally, the IMU token sequence is formed by interleaving product-code indices over time, $\mathbf{s} = [\kappa_{1,1}, \dots, \kappa_{1,P}, \kappa_{2,1}, \dots, \kappa_{T',P}]$. These discrete tokens preserve the temporal order of the setup-stable motion latent and serve as the IMU input tokens for motion-language alignment in Section 3.3. Since both \mathcal{G}_θ and the tokenizer operate temporally, variable-length IMU windows are handled by producing variable-length token sequences.

3.3 Motion-Language Modeling

The tokenizer in Section 3.2 converts sparse wearable observations into discrete IMU token sequences, but these new tokens are not yet meaningful to a pretrained LLM. We therefore use motion language model pre-training to introduce the IMU vocabulary into the LLM and teach the model to understand wearable motion tokens. Multi-task contrastive instruction tuning aligns IMU-token prompts with language descriptions and activity-label prompts for retrieval, captioning, and zero-shot recognition.

Motion Language Model Pre-Training. As shown in Figure 3, with details in Figure 7, motion language model pre-training adapts the LLM to the IMU token vocabulary. We extend the LLM vocabulary with IMU tokens and one code token for each entry in each product codebook. Rather than treating these tokens as unrelated new words, we use the learned tokenizer codebooks to give each IMU token a motion-aware embedding. Specifically, for each IMU code token associated with a codebook vector $\mathbf{e}_{j,k}$, a projector g_ρ maps $\mathbf{e}_{j,k}$ into the LLM embedding space, and the corresponding input embedding is replaced by $g_\rho(\mathbf{e}_{j,k})$ during model execution. The same projected vectors are also used to initialize the corresponding rows in the LM head. We then continue causal LM pre-training on the interleaved IMU token sequence \mathbf{s} using next-token cross-entropy loss $\mathcal{L}_{\text{CE}} = \text{CE}(p(\cdot | s_{<r}), s_r)$.

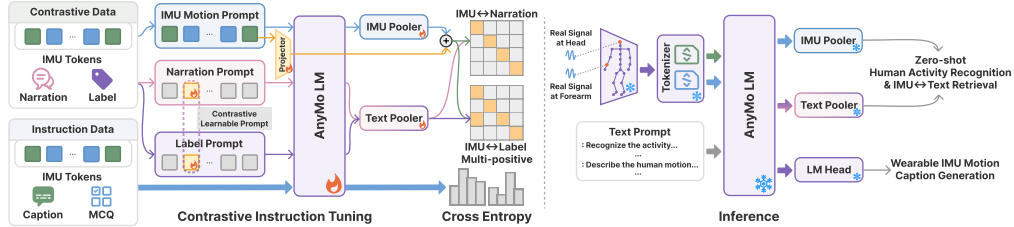


Figure 4: Details of Contrastive Instruction Tuning (left) and inference phases (right) of AnyMo.

Motion Language Multi-Task Contrastive Instruction Tuning. Motion language model pre-training teaches the LLM to read IMU token sequences, but next-token prediction alone does not provide the discriminative motion-language alignment needed by retrieval and zero-shot recognition. At the same time, captioning still requires the model to preserve its generative capability. We therefore use multi-task contrastive instruction tuning to jointly support embedding-based and generation-based motion-language tasks [45, 75], as illustrated in Figure 4.

The language supervision comes from Nymeria [40] atomic-action annotations: we use the atomic-action text as motion narration and derive activity-label names from our semi-automatically curated and human-verified ground-truth action labels. To increase linguistic diversity, each motion window is paired with five augmented narrations, as detailed in Section A.4. For each training example, the IMU branch wraps the token sequence \mathbf{s} in a prompt that also describes the visible wearable locations, while the language side contains two supervision branches built on the same text pooler: a

label branch for activity-label names and a narration branch for ground-truth or augmented motion narrations. The shared LLM processes these prompts. Considering the prompt sensitivity of LLM, the narration and label branches prepend a shared learnable soft prompt before LLM processing [38]. The soft-prompt tokens are optimized through the contrastive objectives [62] but are masked out during pooling, serving as contrastively learned context for language-side representations. We analyze this prompt sensitivity in Section E.1. In parallel, we use an instruction-generation branch for captioning and multiple-choice activity recognition. This branch pairs the IMU token sequence \mathbf{s} with natural-language task prompts, such as caption-generation or multiple-choice question instructions, and supervises the target response tokens through the LM head with next-token cross-entropy loss \mathcal{L}_{CE} . The contrastive embeddings are produced by modality-specific lightweight Transformer-style latent-attention poolers [31] and projection heads. Each pooler operates on the relevant IMU-token or text span while masking out unrelated prompt tokens. The resulting IMU embedding lightly incorporates [21] averaged projected code-token embeddings to retain fine-grained motion semantics from the learned IMU codebook, yielding normalized embeddings \mathbf{h}^{imu} and \mathbf{h}^{text} . For a minibatch of N_{batch} paired IMU-narration examples, the symmetric narration-level IMU-text contrastive loss is:

$$\mathcal{L}_{\text{ITC}} = -\frac{1}{2N_{\text{batch}}} \sum_{n=1}^{N_{\text{batch}}} \left[\log \frac{\exp((\mathbf{h}_n^{\text{imu}})^\top \mathbf{h}_n^{\text{text}} / \tau_{\text{ml}})}{\sum_{m=1}^{N_{\text{batch}}} \exp((\mathbf{h}_n^{\text{imu}})^\top \mathbf{h}_m^{\text{text}} / \tau_{\text{ml}})} + \log \frac{\exp((\mathbf{h}_n^{\text{text}})^\top \mathbf{h}_n^{\text{imu}} / \tau_{\text{ml}})}{\sum_{m=1}^{N_{\text{batch}}} \exp((\mathbf{h}_n^{\text{text}})^\top \mathbf{h}_m^{\text{imu}} / \tau_{\text{ml}})} \right], \quad (5)$$

where τ_{ml} is the motion-language contrastive temperature. In addition to narration-level alignment, the label branch encodes activity-label names and applies a supervised label contrastive loss $\mathcal{L}_{\text{label}}$, where all examples with the same normalized activity label are treated as positives. The final objective is $\mathcal{L}_{\text{CIT}} = \lambda_{\text{CE}} \mathcal{L}_{\text{CE}} + \lambda_{\text{ITC}} \mathcal{L}_{\text{ITC}} + \lambda_{\text{label}} \mathcal{L}_{\text{label}}$. We further analyze the contributions of narration contrastive tuning, label contrastive tuning, and the multiple-choice question in the instruction branch in Table 4. At inference time, a real sparse IMU window is converted into IMU tokens with its available wearable locations, and the tuned model is used either through the pooled embeddings for zero-shot recognition and IMU-text retrieval, or through the LM head for motion caption generation.

4 Experiments

We train AnyMo using Nymeria [40], which provides synchronized body mesh/skeleton motion, atomic-action text annotations, and real IMU streams from the head and two wrists. The mesh and skeleton motion are used to simulate dense geometry-aware IMU candidates for pre-training, while real Nymeria IMU streams are used only to estimate device-noise priors and for held-out sim-to-real evaluation. No downstream benchmark dataset is used to train AnyMo. We use Qwen2.5-0.5B as the LLM backbone of AnyMo [51]. We evaluate along three complementary axes: zero-shot activity recognition across 14 unseen wearable datasets, bidirectional IMU-text retrieval, and wearable IMU motion caption generation. At inference time, each sparse IMU window is converted into IMU tokens, and AnyMo uses only these tokens, the visible wearable-location context, and task-specific text prompts. For recognition, the 14 completely unseen datasets [54, 3, 5, 60, 73, 19, 74, 53, 77, 68, 2, 11, 18, 69] cover diverse body locations, devices, sampling protocols, and activity vocabularies, including four large-scale in-the-wild datasets. We group them by label space size into easy (<10 classes), medium (10–20 classes), and hard (>20 classes) settings. For retrieval and captioning, we evaluate sim-to-real transfer on held-out Nymeria subjects and OOD zero-shot transfer to EgoExo4D. We compare against sensor-language multimodal methods [16, 44, 78], synthetic IMU pre-training methods [32, 78], wearable foundation model [39], and multimodal LLM baselines [27, 49, 17]. We report Accuracy, macro-F1, and Recall@2 for recognition; Recall@K and MRR for retrieval; and BLEU, ROUGE-L, METEOR, and BERT-F1 for captioning. Full dataset statistics, preprocessing, prompt templates, and baseline details are provided in Appendix A, Appendix C, and Appendix D. Separately, Appendix B describes AnyMo Bench, an additional in-the-wild HAR benchmark built from our curated Nymeria activity labels for fine-grained unseen-subject and cross-device recognition.

Zero-shot Human Activity Recognition. Table 1 summarizes zero-shot activity recognition on 14 completely unseen wearable datasets. AnyMo achieves the best average performance across all three metrics, with 35.7 Accuracy, 29.5 macro-F1, and 57.5 Recall@2, improving over the strongest

Table 1: Zero-shot HAR comparison. The best is in **bold**, while the second-best is underlined.

Method	Dataset	Metrics	Opportunity	UCI-HAR	w-HAR	RealWorld	TNDA-HAR	EgoExo4D	OpenPack	PAMAP2	USC-HAD	WISDM	DSADS	UTD-MHAD	Ego4D	MMEA	Average
Number of Classes			4	6	7	8	8	8	10	12	12	18	19	27	31	32	
Level			Easy					Medium					Hard			Average	
ImageBind	Acc	<u>59.3</u>	14.0	8.2	17.4	22.6	8.2	<u>11.6</u>	12.8	11.2	6.9	6.2	2.3	2.8	4.1		13.4
	F1	39.6	6.7	6.1	10.4	18.6	8.5	8.3	7.7	6.9	4.4	3.6	0.8	0.8	1.3		8.8
	R@2	<u>83.5</u>	20.2	52.5	27.4	35.3	12.5	20.7	15.5	23.5	13.5	8.2	4.7	6.4	7.6		23.7
IMU2CLIP	Acc	47.3	30.1	36.1	27.3	26.8	10.9	9.5	14.0	14.8	12.4	11.5	3.7	1.8	5.3		18.0
	F1	37.6	<u>27.3</u>	20.9	20.5	22.3	5.9	4.5	11.3	11.6	8.3	8.3	0.4	0.4	<u>3.1</u>		13.0
	R@2	69.0	55.1	60.7	43.9	46.2	18.5	19.5	26.6	29.1	20.4	17.6	7.9	3.1	<u>10.8</u>		30.6
IMUGPT	Acc	10.1	1.1	67.2	16.9	14.3	12.5	11.4	8.9	6.0	8.3	7.5	3.7	4.6	3.4		12.6
	F1	10.4	0.3	38.8	4.0	6.1	7.6	<u>9.1</u>	1.5	6.9	6.6	2.0	0.3	1.9	1.8		7.0
	R@2	33.7	18.2	<u>67.2</u>	33.7	28.5	27.4	<u>22.9</u>	19.3	31.8	13.9	14.6	8.8	<u>9.3</u>	6.7		24.0
HARGPT	Acc	28.8	15.0	4.9	12.7	13.7	16.1	10.2	11.1	9.5	5.5	5.8	3.3	3.6	2.4		10.2
	F1	17.3	12.7	3.1	5.3	5.4	12.0	5.5	2.1	3.6	3.5	3.4	1.5	1.1	0.9		5.5
	R@2	47.0	31.4	11.5	31.7	25.2	32.0	22.7	23.0	17.6	11.8	12.1	9.3	7.8	6.3		20.7
UniMTS	Acc	45.9	<u>35.2</u>	<u>59.0</u>	<u>43.6</u>	<u>59.1</u>	23.1	11.5	<u>47.2</u>	<u>30.5</u>	27.8	<u>31.5</u>	22.8	3.7	6.1		31.9
	F1	<u>42.2</u>	22.0	42.9	<u>36.7</u>	53.7	18.4	7.5	43.6	27.8	25.5	<u>23.7</u>	18.5	<u>4.3</u>	2.8		<u>26.4</u>
	R@2	80.0	53.1	60.7	<u>64.0</u>	<u>77.5</u>	<u>47.0</u>	21.9	<u>63.2</u>	45.4	47.1	<u>46.0</u>	32.6	6.9	10.7		<u>46.9</u>
NormWear	Acc	26.0	3.7	3.3	16.8	12.2	10.5	9.8	7.9	8.7	4.4	0.7	3.7	2.0	2.7		8.0
	F1	10.3	1.6	1.3	3.8	2.8	3.1	3.1	1.6	1.4	0.9	0.1	0.3	0.2	0.3		2.2
	R@2	66.1	29.6	3.3	20.4	19.1	20.2	16.5	10.5	12.2	12.4	2.6	7.4	5.8	6.0		16.6
Gemma 4 26B _{Text}	Acc	35.9	29.4	29.5	30.8	28.2	18.0	9.6	13.3	29.7	11.6	10.7	4.7	2.4	5.6		18.5
	F1	23.5	19.9	12.7	18.8	19.3	11.8	7.6	7.4	12.4	8.0	7.6	2.0	1.2	1.9		11.0
	R@2	68.4	<u>60.5</u>	31.1	58.9	53.1	40.7	19.4	31.1	42.7	20.8	22.0	10.2	6.7	9.4		33.9
Gemma 4 26B _{Plot}	Acc	39.8	29.8	27.9	31.2	27.8	<u>24.8</u>	7.7	19.4	32.9	9.4	11.5	5.6	3.5	4.4		19.7
	F1	33.0	21.6	10.6	23.6	15.1	11.9	4.5	10.8	14.0	6.1	7.5	1.2	1.3	2.0		11.7
	R@2	74.4	59.6	32.8	58.1	50.1	24.8	18.2	35.4	<u>46.8</u>	16.9	21.5	10.7	7.9	7.9		33.2
AnyMo	Acc	59.4	56.5	57.4	48.4	59.4	30.2	13.1	52.6	27.7	<u>25.4</u>	36.3	<u>16.3</u>	8.6	8.1		35.7(+11.7%)
	F1	58.8	51.6	<u>42.2</u>	37.2	<u>53.1</u>	24.1	11.6	<u>41.5</u>	<u>22.6</u>	<u>18.6</u>	29.5	<u>11.3</u>	6.3	4.0		29.5(+11.6%)
	R@2	83.5	89.5	98.4	77.6	87.9	51.6	28.0	78.2	64.0	<u>41.1</u>	53.0	<u>24.2</u>	13.7	13.9		57.5(+22.6%)

average baseline by 11.7%, 11.6%, and 22.6%, respectively. The gains hold across controlled HAR benchmarks and in the wild datasets, suggesting that AnyMo learns transferable motion-language representations. ImageBind and IMU2CLIP provide sensor-language multimodal alignment and perform competitively on a few low-class datasets, but their performance drops as sensing setups and label spaces become more diverse. IMUGPT and UniMTS benefit from synthetic IMU motion pre-training, with UniMTS serving as the strongest prior baseline across the benchmark. AnyMo further improves over them through geometry-aware surface simulation and pre-training, and motion-language alignment. HARGPT and the Gemma 4 26B prompting baselines test whether substantially larger LLM priors alone can support zero-shot HAR: HARGPT uses role-play and step-by-step prompts over raw IMU readings, while Gemma 4 26B uses numerical IMU input or plots of IMU readings for multimodal understanding. The Gemma 4 26B prompting baselines occasionally perform well on individual datasets, but remain substantially below AnyMo on average, indicating that direct language or vision-language prompting, even at larger scale, is not sufficient for robust cross-setup wearable motion recognition. NormWear, despite pre-training on heterogeneous physiological and inertial signals including IMU, performs weakly in this benchmark. Suggesting that broad wearable-signal pre-training alone does not directly transfer to language-grounded open-vocabulary HAR across diverse unseen datasets and body placements.

Cross-Modal Retrieval. Table 2 evaluates bidirectional retrieval between sparse IMU windows and motion narrations. The Nymeria held-out split is designed as a synthetic-to-real transfer test: AnyMo is trained without the held-out subjects using synthetic IMU candidates generated from body mesh/skeleton motion, while all methods are evaluated on the same real IMU streams from held-out subjects. ImageBind and IMU2CLIP reflect large-scale real sensor-language pre-training, UniMTS reflects an alternative synthetic IMU pre-training strategy, and GPT-5.4 Mini/Gemma 4 26B test whether much larger state-of-the-art LLMs can solve retrieval through prompting. AnyMo

Table 2: Unseen and zero-shot cross-modal retrieval performance on Nymeria held-out set and EgoExo4D datasets. “–” denotes settings infeasible for LLM baselines due to context-length limits.

Dataset		Nymeria Held-out								EgoExo4D Zero-shot							
Task	Method	100 Samples				All Samples				100 Samples				All Samples			
		R@1	R@5	R@10	MRR	R@1	R@5	R@10	MRR	R@1	R@5	R@10	MRR	R@1	R@5	R@10	MRR
IMU ↓ Text	ImageBind	0.0	6.0	14.0	5.0	0.1	0.2	0.3	0.3	1.0	5.0	8.0	4.6	0.1	0.2	0.3	0.3
	IMU2CLIP	1.0	6.0	12.0	5.5	0.0	0.1	0.3	0.3	2.0	10.0	23.0	8.2	0.0	0.3	0.5	0.4
	UniMTS	4.0	12.0	23.0	10.0	0.2	0.9	1.6	0.9	1.0	9.0	16.0	6.3	0.1	0.6	1.3	0.7
	GPT-5.4 Mini	1.0	7.0	11.0	4.4	–	–	–	–	1.0	6.0	10.0	3.7	–	–	–	–
	Gemma 4 26B	2.0	9.0	16.0	6.1	–	–	–	–	2.0	4.0	12.0	4.6	–	–	–	–
	AnyMo	28.0	63.0	77.0	44.6	2.3	9.5	15.4	7.0	2.0	9.0	27.0	9.5	0.2	0.7	1.4	0.8
Text ↓ IMU	ImageBind	1.0	8.0	14.0	6.7	0.1	0.2	0.3	0.3	2.0	3.0	7.0	5.1	0.0	0.0	0.2	0.2
	IMU2CLIP	0.0	6.0	14.0	5.0	0.1	0.2	0.3	0.3	1.0	9.0	17.0	7.7	0.1	0.3	0.5	0.4
	UniMTS	1.0	6.0	12.0	5.5	0.1	0.2	0.4	0.3	1.0	5.0	10.0	5.3	0.0	0.1	0.3	0.2
	GPT-5.4 Mini	–	–	–	–	–	–	–	–	–	–	–	–	–	–	–	–
	Gemma 4 26B	–	–	–	–	–	–	–	–	–	–	–	–	–	–	–	–
	AnyMo	33.0	60.0	79.0	46.7	3.0	9.9	16.1	7.5	3.0	10.0	23.0	9.9	0.0	0.3	0.6	0.4

substantially outperforms all baselines on Nymeria held-out, improving 100-sample IMU→Text MRR from 10.0 to 44.6 and Text→IMU MRR from 6.7 to 46.7, while remaining clearly ahead in the harder all-sample setting. EgoExo4D further evaluates OOD zero-shot transfer. Although all methods degrade, AnyMo achieves the best or second-best performance on most metrics.

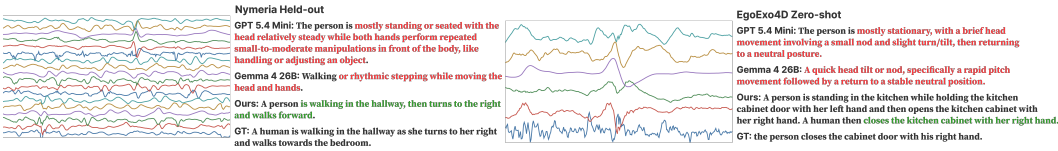


Figure 5: Qualitative Results of Wearable IMU Motion Caption Generation. We use green to highlight correct parts and red for mistakes.

Wearable IMU Motion Captioning. Table 3 evaluates AnyMo’s generative motion-language capability. Under the same Nymeria held-out and EgoExo4D zero-shot settings, AnyMo outperforms GPT-5.4 Mini and Gemma 4 26B across captioning metrics. On Nymeria held-out, AnyMo substantially improves over the strongest prompting baseline, increasing ROUGE-L from 15.7 to 31.1 and BERT-F1 from 57.3 to 69.7. These gains show that the learned IMU tokens retain motion semantics that can be decoded into natural-language descriptions. The advantage persists under EgoExo4D zero-shot transfer, where AnyMo achieves 20.7 BLEU-1, 30.3 METEOR, and 67.1 BERT-F1 despite OOD motion distributions. This suggests that AnyMo provides stronger generative modeling than direct LLM prompting over IMU observations. Figure 5 provides qualitative examples. The prompting baselines often describe generic posture changes or local signal fluctuations, such as standing, head motion, or hand movement, while missing the full activity. In contrast, AnyMo produces captions that better preserve the action-level semantics, including walking direction changes in Nymeria and cabinet-closing interactions in EgoExo4D. These results suggest that the IMU tokenizer and motion-language instruction tuning enable open-ended motion description from wearable signals.

Table 3: Unseen and zero-shot IMU motion caption generation results on Nymeria and EgoExo4D.

Dataset	Nymeria Held-out					EgoExo4D Zero-shot				
	Method	BLEU-1	BLEU-4	ROUGE-L	METEOR	BERT-F1	BLEU-1	BLEU-4	ROUGE-L	METEOR
GPT-5.4 Mini	19.2	0.3	15.7	25.0	57.3	12.6	0.0	15.5	23.8	56.5
Gemma 4 26B	16.2	0.0	13.6	21.5	56.5	3.5	0.0	4.6	6.4	55.1
AnyMo	25.0	6.5	31.1	33.5	69.7	20.7	0.4	19.7	30.3	67.1

Ablation. Table 4 ablates each component (see Section A.8 for detailed implementation). Removing geometry-aware simulation causes the largest degradation, reducing performance from 35.7/29.5/57.5 to 8.4/3.8/16.3 in Acc/F1/R@2. Replacing the masked cross-view predictive contrastive objective also severely hurts performance. These results indicate that synthetic IMU generation alone is insufficient: the model needs both realistic surface-aware setup variation and a

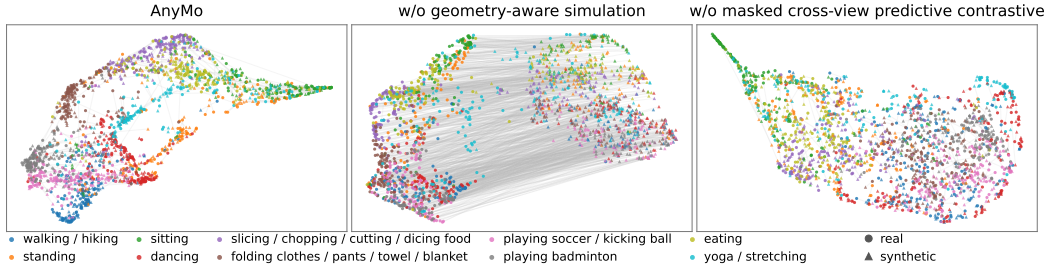


Figure 6: UMAP visualization of paired real and synthetic IMU embeddings for ten activity categories.

sparse-to-full pre-training objective to transfer from synthetic full-body candidates to real sparse wearable inputs. Figure 6 further visualizes this effect. For 10 activity categories, we randomly sample 100 real and 100 synthetic windows per activity and plot their embeddings with UMAP [42]. AnyMo forms more discriminative activity clusters while aligning real and synthetic samples of the same activity. Without geometry-aware simulation, real and synthetic embeddings separate by domain, while removing masked cross-view predictive contrastive learning reduces cluster coherence, highlighting the importance of both components for synthetic-to-real alignment. The motion-language losses are also important. Removing label or narration contrastive tuning degrades Acc, F1, and R@2, showing that both label-level supervision and free-form narration alignment support zero-shot recognition. Removing all contrastive tuning further degrades performance, confirming that next-token instruction tuning alone is insufficient for discriminative open-vocabulary recognition. Finally, removing MCQ instruction tuning slightly increases Acc but reduces F1 and R@2, suggesting that the MCQ branch mainly improves balanced recognition and candidate ranking.

Table 4: Ablation study.

Variant	Acc	F1	R@2
AnyMo	35.7	29.5	57.5
<i>Simulation and encoder pretraining</i>			
w/o geometry-aware simulation	8.4	3.8	16.3
w/o masked cross-view pred. contrastive	10.5	4.5	19.0
<i>Motion-language contrastive</i>			
w/o label contrastive	33.3	27.1	51.4
w/o narration contrastive	32.6	23.8	50.1
w/o all contrastive	23.5	15.8	40.3
<i>LM instruction tuning</i>			
w/o MCQ instruction tuning	36.0	29.4	54.6

5 Conclusion

We presented AnyMo, a geometry-aware setup-agnostic framework for wearable IMU motion understanding under variable sensing setups. AnyMo treats wearable setup variation as structured body-surface variation, synthesizes dense physics-grounded IMU candidates from human mesh motion, learns setup-agnostic full-body motion representations, and connects them to language models through compact full-body IMU tokens. Across zero-shot activity recognition, bidirectional IMU-text retrieval, and wearable motion caption generation, AnyMo shows consistent gains on unseen datasets, held-out real Nymeria IMU streams, and out-of-domain EgoExo4D transfer. These results suggest that combining geometry-aware wearable simulation with motion-language modeling is a promising path toward generalist motion understanding from sparse wearable sensors.

Acknowledgments and Disclosure of Funding

This research includes computations using the Wolfpack computational cluster, supported by the School of Computer Science and Engineering at UNSW Sydney. We also acknowledge support from the ARC Centre of Excellence for Automated Decision-Making and Society (CE200100005).

References

[1] J.K. Aggarwal and M.S. Ryoo. Human activity analysis: A review. *ACM Comput. Surv.*, 43(3), April 2011. ISSN 0360-0300. doi: 10.1145/1922649.1922653.

- [2] Kerem Altun, Billur Barshan, and Orkun Tunçel. Comparative study on classifying human activities with miniature inertial and magnetic sensors. *Pattern Recognition*, 43(10):3605–3620, 2010.
- [3] Davide Anguita, Alessandro Ghio, Luca Oneto, Xavier Parra, Jorge Luis Reyes-Ortiz, et al. A public domain dataset for human activity recognition using smartphones. In *Esann*, volume 3, pages 3–4, 2013.
- [4] Sheikh Asif Imran Shouborno, Mohammad Nur Hossain Khan, Subrata Biswas, and Bashima Islam. Llasa: A sensor-aware llm for natural language reasoning of human activity from imu data. In *Companion of the 2025 ACM International Joint Conference on Pervasive and Ubiquitous Computing, UbiComp Companion '25*, page 893–899, New York, NY, USA, 2025. Association for Computing Machinery. ISBN 9798400714771. doi: 10.1145/3714394.3756187.
- [5] Ganapati Bhat, Nicholas Tran, Holly Shill, and Umit Y Ogras. w-har: An activity recognition dataset and framework using low-power wearable devices. *Sensors*, 20(18):5356, 2020.
- [6] Sizhen Bian, Mengxi Liu, Siyu Yuan, Lala Shakti Swarup Ray, Bo Zhou, Bin Guo, Zhiwen Yu, Thomas Ploetz, Paul Lukowicz, and Vitor Fortes Rey. Foundation models defining a new era in sensor-based human activity recognition: A survey and outlook. *arXiv preprint arXiv:2604.02711*, 2026.
- [7] Andreas Bulling, Ulf Blanke, and Bernt Schiele. A tutorial on human activity recognition using body-worn inertial sensors. *ACM Comput. Surv.*, 46(3), January 2014. ISSN 0360-0300. doi: 10.1145/2499621.
- [8] Yize Cai, Baoshen Guo, Flora Salim, and Zhiqing Hong. Towards generalizable human activity recognition: A survey. *arXiv preprint arXiv:2508.12213*, 2025.
- [9] Youngjae Chang, Akhil Mathur, Anton Isopoussu, Junehwa Song, and Fahim Kawsar. A systematic study of unsupervised domain adaptation for robust human-activity recognition. *Proc. ACM Interact. Mob. Wearable Ubiquitous Technol.*, 4(1), March 2020. doi: 10.1145/3380985.
- [10] Baiyu Chen, Wilson Wongso, Zechen Li, Yonchanok Khaokaew, Hao Xue, and Flora Salim. Comodo: Cross-modal video-to-imu distillation for efficient egocentric human activity recognition. *arXiv preprint arXiv:2503.07259*, 2025.
- [11] Chen Chen, Roozbeh Jafari, and Nasser Kehtarnavaz. Utd-mhad: A multimodal dataset for human action recognition utilizing a depth camera and a wearable inertial sensor. In *2015 IEEE International conference on image processing (ICIP)*, pages 168–172. IEEE, 2015.
- [12] Anind K Dey. Understanding and using context. *Personal and ubiquitous computing*, 5(1):4–7, 2001.
- [13] Vasilii Feofanov, Songkang Wen, Jianfeng Zhang, Lujia Pan, and Ievgen Redko. Mantisv2: Closing the zero-shot gap in time series classification with synthetic data and test-time strategies. *arXiv preprint arXiv:2602.17868*, 2026.
- [14] Vitor Fortes Rey, Sungho Suh, and Paul Lukowicz. Learning from the best: Contrastive representations learning across sensor locations for wearable activity recognition. ISWC '22, page 28–32, New York, NY, USA, 2022. Association for Computing Machinery. ISBN 9781450394246. doi: 10.1145/3544794.3558464.
- [15] Luyu Gao, Yunyi Zhang, Jiawei Han, and Jamie Callan. Scaling deep contrastive learning batch size under memory limited setup. In Anna Rogers, Iacer Calixto, Ivan Vulić, Naomi Saphra, Nora Kassner, Oana-Maria Camburu, Trapit Bansal, and Vered Shwartz, editors, *Proceedings of the 6th Workshop on Representation Learning for NLP (RepL4NLP-2021)*, pages 316–321, Online, August 2021. Association for Computational Linguistics. doi: 10.18653/v1/2021.repl4nlp-1.31.
- [16] Rohit Girdhar, Alaaeldin El-Nouby, Zhuang Liu, Mannat Singh, Kalyan Vasudev Alwala, Armand Joulin, and Ishan Misra. ImageBind: One embedding space to bind them all. In *Proceedings of the IEEE/CVF Conference on Computer Vision and Pattern Recognition*, pages 15180–15190, 2023.

- [17] Google DeepMind. Gemma 4 Model Card. Technical report, April 2026. Last updated: 2026-04-17.
- [18] Kristen Grauman, Andrew Westbury, Eugene Byrne, Zachary Chavis, Antonino Furnari, Rohit Girdhar, Jackson Hamburger, Hao Jiang, Miao Liu, Xingyu Liu, Miguel Martin, et al. Ego4D: Around the world in 3,000 hours of egocentric video. In *Proceedings of the IEEE/CVF Conference on Computer Vision and Pattern Recognition*, pages 18995–19012, 2022.
- [19] Kristen Grauman, Andrew Westbury, Lorenzo Torresani, Kris Kitani, Jitendra Malik, Triantafyllos Afouras, Kumar Ashutosh, Vijay Baiyya, Siddhant Bansal, Bikram Boote, et al. Ego-exo4d: Understanding skilled human activity from first-and third-person perspectives. In *Proceedings of the IEEE/CVF Conference on Computer Vision and Pattern Recognition*, pages 19383–19400, 2024.
- [20] Harish Haresamudram, Chi Ian Tang, Sungho Suh, Paul Lukowicz, and Thomas Plötz. Past, present, and future of sensor-based human activity recognition using wearables: A surveying tutorial on a still challenging task. *Proc. ACM Interact. Mob. Wearable Ubiquitous Technol.*, 9(2), June 2025. doi: 10.1145/3729467.
- [21] Kaiming He, Xiangyu Zhang, Shaoqing Ren, and Jian Sun. Deep residual learning for image recognition. In *Proceedings of the IEEE conference on computer vision and pattern recognition*, pages 770–778, 2016.
- [22] Pengcheng He, Xiaodong Liu, Jianfeng Gao, and Weizhu Chen. {DEBERTA}: {DECODING}-{enhanced} {bert} {with} {disentangled} {attention}. In *International Conference on Learning Representations*, 2021. URL <https://openreview.net/forum?id=XPZLaotutsD>.
- [23] Fangzhou Hong, Vladimir Guzov, Hyo Jin Kim, Yuting Ye, Richard Newcombe, Ziwei Liu, and Lingni Ma. Ego4m: Multi-modal language model of egocentric motions. In *Proceedings of the Computer Vision and Pattern Recognition Conference*, pages 5344–5354, 2025.
- [24] Zhiqing Hong, Zelong Li, Shuxin Zhong, Wenjun Lyu, Haotian Wang, Yi Ding, Tian He, and Desheng Zhang. Crosshar: Generalizing cross-dataset human activity recognition via hierarchical self-supervised pretraining. *Proc. ACM Interact. Mob. Wearable Ubiquitous Technol.*, 8(2), May 2024. doi: 10.1145/3659597.
- [25] Zhenyu Hou, Yufei He, Yukuo Cen, Xiao Liu, Yuxiao Dong, Evgeny Kharlamov, and Jie Tang. Graphmae2: A decoding-enhanced masked self-supervised graph learner. In *Proceedings of the ACM web conference 2023*, pages 737–746, 2023.
- [26] Xiaohu Huang, Hao Zhou, Jian Wang, Haocheng Feng, Junyu Han, Errui Ding, Jingdong Wang, Xinggong Wang, Wenyu Liu, and Bin Feng. Graph contrastive learning for skeleton-based action recognition. In *The Eleventh International Conference on Learning Representations*, 2023. URL <https://openreview.net/forum?id=PLUXnnxUdr4>.
- [27] Sijie Ji, Xinzhe Zheng, and Chenshu Wu. HARGPT: Are LLMs zero-shot human activity recognizers? In *2024 IEEE International Workshop on Foundation Models for Cyber-Physical Systems & Internet of Things (FMSys)*, pages 38–43, 2024. doi: 10.1109/FMSys62467.2024.00011.
- [28] Biao Jiang, Xin Chen, Wen Liu, Jingyi Yu, Gang Yu, and Tao Chen. Motiongpt: Human motion as a foreign language. *Advances in Neural Information Processing Systems*, 36:20067–20079, 2023.
- [29] Kaleab A Kinfe and Rene Vidal. Motionbind: Multi-modal human motion alignment for retrieval, recognition, and generation. In *The Thirty-ninth Annual Conference on Neural Information Processing Systems*, 2025. URL <https://openreview.net/forum?id=sUjwDdyspc>.
- [30] Kai Kunze and Paul Lukowicz. Sensor placement variations in wearable activity recognition. *IEEE Pervasive Computing*, 13(4):32–41, 2014. doi: 10.1109/MPRV.2014.73.

- [31] Chankyu Lee, Rajarshi Roy, Mengyao Xu, Jonathan Raiman, Mohammad Shoeybi, Bryan Catanzaro, and Wei Ping. NV-embed: Improved techniques for training LLMs as generalist embedding models. In *The Thirteenth International Conference on Learning Representations*, 2025. URL <https://openreview.net/forum?id=lgsyLSsDRe>.
- [32] Zikang Leng, Hyeokhyen Kwon, and Thomas Ploetz. Generating virtual on-body accelerometer data from virtual textual descriptions for human activity recognition. In *Proceedings of the 2023 ACM International Symposium on Wearable Computers, ISWC '23*, page 39–43, New York, NY, USA, 2023. Association for Computing Machinery. ISBN 9798400701993. doi: 10.1145/3594738.3611361.
- [33] Zikang Leng, Amitrajit Bhattacharjee, Hrudhai Rajasekhar, Lizhe Zhang, Elizabeth Bruda, Hyeokhyen Kwon, and Thomas Plötz. Imugpt 2.0: Language-based cross modality transfer for sensor-based human activity recognition. *Proc. ACM Interact. Mob. Wearable Ubiquitous Technol.*, 8(3), September 2024. doi: 10.1145/3678545.
- [34] Linguo Li, Minsi Wang, Bingbing Ni, Hang Wang, Jiancheng Yang, and Wenjun Zhang. 3d human action representation learning via cross-view consistency pursuit. In *Proceedings of the IEEE/CVF conference on computer vision and pattern recognition*, pages 4741–4750, 2021.
- [35] Zechen Li, Baiyu Chen, Hao Xue, and Flora D Salim. Zara: Training-free motion time-series reasoning via evidence-grounded llm agents. *arXiv preprint arXiv:2508.04038*, 2025.
- [36] Zechen Li, Shohreh Deldari, Linyao Chen, Hao Xue, and Flora D. Salim. SensorLLM: Aligning large language models with motion sensors for human activity recognition. In Christos Christodoulopoulos, Tanmoy Chakraborty, Carolyn Rose, and Violet Peng, editors, *Proceedings of the 2025 Conference on Empirical Methods in Natural Language Processing*, pages 354–379, Suzhou, China, November 2025. Association for Computational Linguistics. ISBN 979-8-89176-332-6. doi: 10.18653/v1/2025.emnlp-main.19. URL <https://aclanthology.org/2025.emnlp-main.19/>.
- [37] Lilang Lin, Jiahang Zhang, and Jiaying Liu. Actionlet-dependent contrastive learning for unsupervised skeleton-based action recognition. In *Proceedings of the IEEE/CVF Conference on Computer Vision and Pattern Recognition*, pages 2363–2372, 2023.
- [38] Xiao Liu, Yanan Zheng, Zhengxiao Du, Ming Ding, Yujie Qian, Zhilin Yang, and Jie Tang. Gpt understands, too. *AI open*, 5:208–215, 2024.
- [39] Yunfei Luo, Yuliang Chen, Asif Salekin, and Tauhidur Rahman. Toward foundation model for multivariate wearable sensing of physiological signals. *ACM Trans. Comput. Healthcare*, March 2026. doi: 10.1145/3803808.
- [40] Lingni Ma, Yuting Ye, Fangzhou Hong, Vladimir Guzov, Yifeng Jiang, Rowan Postyeni, Luis Pesqueira, Alexander Gamino, Vijay Baiyya, Hyo Jin Kim, et al. Nymeria: A massive collection of multimodal egocentric daily motion in the wild. In *European Conference on Computer Vision*, pages 445–465. Springer, 2024.
- [41] Yunyao Mao, Jiajun Deng, Wengang Zhou, Yao Fang, Wanli Ouyang, and Houqiang Li. Masked motion predictors are strong 3d action representation learners. In *Proceedings of the IEEE/CVF International Conference on Computer Vision*, pages 10181–10191, 2023.
- [42] Leland McInnes, John Healy, and James Melville. UMAP: Uniform manifold approximation and projection for dimension reduction. *arXiv preprint arXiv:1802.03426*, 2018. URL <https://arxiv.org/abs/1802.03426>.
- [43] Shenghuan Miao and Ling Chen. Wonderwall: A virtual-to-real foundation model for imu-based har. *Proc. ACM Interact. Mob. Wearable Ubiquitous Technol.*, 10(1), March 2026. doi: 10.1145/3789688.
- [44] Seungwhan Moon, Andrea Madotto, Zhaojiang Lin, Aparajita Saraf, Amy Bearman, and Babak Damavandi. IMU2CLIP: Language-grounded motion sensor translation with multimodal contrastive learning. In Houda Bouamor, Juan Pino, and Kalika Bali, editors, *Findings of the Association for Computational Linguistics: EMNLP 2023*, pages 13246–13253, Singapore, December

2023. Association for Computational Linguistics. doi: 10.18653/v1/2023.findings-emnlp.883. URL <https://aclanthology.org/2023.findings-emnlp.883/>.
- [45] Niklas Muennighoff, Hongjin SU, Liang Wang, Nan Yang, Furu Wei, Tao Yu, Amanpreet Singh, and Douwe Kiela. Generative representational instruction tuning. In *The Thirteenth International Conference on Learning Representations, 2025*. URL <https://openreview.net/forum?id=BC41IvfSzv>.
- [46] Duc Duy Nguyen, Tat-Jun Chin, and Minh Hoai. Mobind: Motion binding for fine-grained imu-video pose alignment. *arXiv preprint arXiv:2602.19004*, 2026.
- [47] Nobuyuki Oishi, Phil Birch, Daniel Roggen, and Paula Lago. Wimusim: simulating realistic variabilities in wearable imus for human activity recognition. *Frontiers in Computer Science*, Volume 7 - 2025, 2025. ISSN 2624-9898. doi: 10.3389/fcomp.2025.1514933. URL <https://www.frontiersin.org/journals/computer-science/articles/10.3389/fcomp.2025.1514933>.
- [48] OpenAI. gpt-oss-120b & gpt-oss-20b Model Card, 2025. URL <https://arxiv.org/abs/2508.10925>.
- [49] OpenAI. GPT-5.4 Thinking System Card. Technical report, OpenAI, March 2026. URL <https://deploymentsafety.openai.com/gpt-5-4-thinking/gpt-5-4-thinking.pdf>. System card.
- [50] Francisco Javier Ordóñez and Daniel Roggen. Deep convolutional and lstm recurrent neural networks for multimodal wearable activity recognition. *Sensors*, 16(1), 2016. ISSN 1424-8220. doi: 10.3390/s16010115. URL <https://www.mdpi.com/1424-8220/16/1/115>.
- [51] Qwen, :, An Yang, Baosong Yang, Beichen Zhang, Binyuan Hui, Bo Zheng, Bowen Yu, Chengyuan Li, Dayiheng Liu, Fei Huang, Haoran Wei, Huan Lin, Jian Yang, Jianhong Tu, Jianwei Zhang, Jianxin Yang, Jiaxi Yang, Jingren Zhou, Junyang Lin, Kai Dang, Keming Lu, Keqin Bao, Kexin Yang, Le Yu, Mei Li, Mingfeng Xue, Pei Zhang, Qin Zhu, Rui Men, Runji Lin, Tianhao Li, Tianyi Tang, Tingyu Xia, Xingzhang Ren, Xuancheng Ren, Yang Fan, Yang Su, Yichang Zhang, Yu Wan, Yuqiong Liu, Zeyu Cui, Zhenru Zhang, and Zihan Qiu. Qwen2.5 technical report. Technical report, 2025. URL <https://arxiv.org/abs/2412.15115>.
- [52] Lala Shakti Swarup Ray, Bo Zhou, and Paul Lukowicz. W2w: A simulated exploration of imu placement across the human body for designing smarter wearable. In *Proceedings of the 2025 ACM International Symposium on Wearable Computers, ISWC '25*, page 170–176, New York, NY, USA, 2025. Association for Computing Machinery. ISBN 9798400714818. doi: 10.1145/3715071.3750417.
- [53] Attila Reiss and Didier Stricker. Introducing a new benchmarked dataset for activity monitoring. In *2012 16th international symposium on wearable computers*, pages 108–109. IEEE, 2012.
- [54] Daniel Roggen, Alberto Calatroni, Mirco Rossi, Thomas Holleczeck, Kilian Förster, Gerhard Tröster, Paul Lukowicz, David Bannach, Gerald Pirkl, Alois Ferscha, et al. Collecting complex activity datasets in highly rich networked sensor environments. In *2010 Seventh international conference on networked sensing systems (INSS)*, pages 233–240. IEEE, 2010.
- [55] Bodo Rosenhahn, Reinhard Klette, and Dimitris Metaxas. Human motion. *Understanding, Modeling, Capture*, 2008.
- [56] Bill Schilit, Norman Adams, and Roy Want. Context-aware computing applications. In *1994 first workshop on mobile computing systems and applications*, pages 85–90. IEEE, 1994.
- [57] Allan Stisen, Henrik Blunck, Sourav Bhattacharya, Thor Siiger Prentow, Mikkel Baun Kjær-gaard, Anind Dey, Tobias Sonne, and Mads Møller Jensen. Smart devices are different: Assessing and mitigating mobile sensing heterogeneities for activity recognition. In *Proceedings of the 13th ACM Conference on Embedded Networked Sensor Systems, SenSys '15*, page 127–140, New York, NY, USA, 2015. Association for Computing Machinery. ISBN 9781450336314. doi: 10.1145/2809695.2809718.

- [58] Marcin Straczekiewicz, Peter James, and Jukka-Pekka Onnela. A systematic review of smartphone-based human activity recognition methods for health research. *npj Digital Medicine*, 4(1):148, 2021. ISSN 2398-6352. doi: 10.1038/s41746-021-00514-4. URL <https://doi.org/10.1038/s41746-021-00514-4>.
- [59] Jie Su, Fengtong Ge, Zhenyu Wen, Taotao Li, Yang Bai, Yejian Zhou, and Xiaoqin Zhang. Imuzero: Zero-shot human activity recognition by language-based cross modality fusion. *Proc. ACM Interact. Mob. Wearable Ubiquitous Technol.*, 9(4), December 2025. doi: 10.1145/3770669.
- [60] Timo Sztyler and Heiner Stuckenschmidt. On-body localization of wearable devices: An investigation of position-aware activity recognition. In *2016 IEEE international conference on pervasive computing and communications (PerCom)*, pages 1–9. IEEE, 2016.
- [61] Timo Sztyler and Heiner Stuckenschmidt. On-body localization of wearable devices: An investigation of position-aware activity recognition. In *2016 IEEE International Conference on Pervasive Computing and Communications (PerCom)*, pages 1–9, 2016. doi: 10.1109/PERCOM.2016.7456521.
- [62] Yue Tan, Xiaoqian Hu, Hao Xue, Celso M de Melo, and Flora D. Salim. Bisecle: Binding and separation in continual learning for video language understanding. In *The Thirty-ninth Annual Conference on Neural Information Processing Systems, 2025*. URL <https://openreview.net/forum?id=o6keqobP13>.
- [63] Catherine Tong, Jincheng Ge, and Nicholas D. Lane. Zero-shot learning for imu-based activity recognition using video embeddings. *Proc. ACM Interact. Mob. Wearable Ubiquitous Technol.*, 5(4), December 2022. doi: 10.1145/3494995.
- [64] Ashish Vaswani, Noam Shazeer, Niki Parmar, Jakob Uszkoreit, Llion Jones, Aidan N Gomez, Łukasz Kaiser, and Illia Polosukhin. Attention is all you need. *Advances in neural information processing systems*, 30, 2017.
- [65] Chongyang Wang, Yuan Feng, Lingxiao Zhong, Siyi Zhu, Chi Zhang, Siqi Zheng, Chen Liang, Yuntao Wang, Chengqi He, Chun Yu, and Yuanchun Shi. Ubiphysio: Support daily functioning, fitness, and rehabilitation with action understanding and feedback in natural language. *Proc. ACM Interact. Mob. Wearable Ubiquitous Technol.*, 8(1), March 2024. doi: 10.1145/3643552.
- [66] Jian Wang, Rishabh Dabral, Diogo Luvizon, Zhe Cao, Lingjie Liu, Thabo Beeler, and Christian Theobalt. Ego4o: Egocentric human motion capture and understanding from multi-modal input. In *Proceedings of the Computer Vision and Pattern Recognition Conference*, pages 22668–22679, 2025.
- [67] Qingxin Wei, Jiaming Huang, Yi Gao, and Wei Dong. One model to fit them all: Universal imu-based human activity recognition with llm-assisted cross-dataset representation. *Proc. ACM Interact. Mob. Wearable Ubiquitous Technol.*, 9(3), September 2025. doi: 10.1145/3749509.
- [68] Gary M Weiss. Wism smartphone and smartwatch activity and biometrics dataset. *UCI Machine Learning Repository: WISDM Smartphone and Smartwatch Activity and Biometrics Dataset Data Set*, 7(133190-133202):5, 2019.
- [69] Linfeng Xu, Qingbo Wu, Lili Pan, Fanman Meng, Hongliang Li, Chiyuan He, Hanxin Wang, Shaoxu Cheng, and Yu Dai. Towards continual egocentric activity recognition: A multi-modal egocentric activity dataset for continual learning. *IEEE Transactions on Multimedia*, 26: 2430–2443, 2024. doi: 10.1109/TMM.2023.3295899.
- [70] Maxwell A Xu, Jaya Narain, Gregory Darnell, Haraldur T Hallgrímsson, Hyewon Jeong, Darren Forde, Richard Andres Fineman, Karthik Jayaraman Raghuram, James Matthew Rehg, and Shirley You Ren. Relcon: Relative contrastive learning for a motion foundation model for wearable data. In *The Thirteenth International Conference on Learning Representations, 2025*. URL <https://openreview.net/forum?id=k2uUeLCrQq>.
- [71] Hong Yan, Yang Liu, Yushen Wei, Zhen Li, Guanbin Li, and Liang Lin. Skeletonmae: graph-based masked autoencoder for skeleton sequence pre-training. In *Proceedings of the IEEE/CVF international conference on computer vision*, pages 5606–5618, 2023.

- [72] Sijie Yan, Yuanjun Xiong, and Dahua Lin. Spatial temporal graph convolutional networks for skeleton-based action recognition. In *Proceedings of the AAAI conference on artificial intelligence*, volume 32, 2018.
- [73] Yan Yan, Dali Chen, Yushi Liu, Jinjin Zhao, Bo Wang, Xuankun Wu, Xiaohao Jiao, Yuqian Chen, Huihui Li, and Xuchao Ren. Tnda-har, 2021. URL <https://dx.doi.org/10.21227/4epb-pg26>.
- [74] Naoya Yoshimura, Jaime Morales, Takuya Maekawa, and Takahiro Hara. Openpack: A large-scale dataset for recognizing packaging works in iot-enabled logistic environments. In *2024 IEEE International Conference on Pervasive Computing and Communications (PerCom)*, pages 90–97, 2024. doi: 10.1109/PerCom59722.2024.10494448.
- [75] Hao Yu, Zhuokai Zhao, Shen Yan, Lukasz Korycki, Jianyu Wang, Baosheng He, Jiayi Liu, Lizhu Zhang, Xiangjun Fan, and Hanchao Yu. Cafe: Unifying representation and generation with contrastive-autoregressive finetuning. In *Proceedings of the IEEE/CVF International Conference on Computer Vision*, pages 6286–6297, 2025.
- [76] Hao Zhang, Zhan Zhuang, Xuehao Wang, Xiaodong Yang, and Yu Zhang. MoPFormer: Motion-primitive transformer for wearable-sensor activity recognition. In *The Thirty-ninth Annual Conference on Neural Information Processing Systems*, 2025. URL <https://openreview.net/forum?id=Ty9n72fZ1K>.
- [77] Mi Zhang and Alexander A Sawchuk. Usc-had: A daily activity dataset for ubiquitous activity recognition using wearable sensors. In *Proceedings of the 2012 ACM conference on ubiquitous computing*, pages 1036–1043, 2012.
- [78] Xiyuan Zhang, Diyan Teng, Ranak R Chowdhury, Shuheng Li, Dezhi Hong, Rajesh K Gupta, and Jingbo Shang. Unimts: Unified pre-training for motion time series. *Advances in Neural Information Processing Systems*, 37:107469–107493, 2024.
- [79] Yanzhao Zhang, Mingxin Li, Dingkun Long, Xin Zhang, Huan Lin, Baosong Yang, Pengjun Xie, An Yang, Dayiheng Liu, Junyang Lin, Fei Huang, and Jingren Zhou. Qwen3 Embedding: Advancing text embedding and reranking through foundation models. *arXiv preprint arXiv:2506.05176*, 2025. URL <https://arxiv.org/abs/2506.05176>.
- [80] Yuwei Zhang, Kumar Ayush, Siyuan Qiao, A. Ali Heydari, Girish Narayanswamy, Maxwell A Xu, Ahmed Metwally, Jinhua Xu, Jake Garrison, Xuhai Xu, Tim Althoff, Yun Liu, Pushmeet Kohli, Jiening Zhan, Mark Malhotra, Shwetak Patel, Cecilia Mascolo, Xin Liu, Daniel McDuff, and Yuzhe Yang. SensorLM: Learning the language of wearable sensors. In *The Thirty-ninth Annual Conference on Neural Information Processing Systems*, 2025. URL <https://openreview.net/forum?id=TrHeq0yFhv>.
- [81] Yuze Zhao, Jiaying Huang, Junjie Hu, Xintao Wang, Yuxuan Mao, Dingkan Zhang, Zhenyu Jiang, Ziyi Wu, Bin Ai, Ang Wang, and Wen Zhou. SWIFT: A scalable lightweight infrastructure for fine-tuning. In *Proceedings of the AAAI Conference on Artificial Intelligence*, volume 39, pages 29733–29735, 2025.
- [82] Chuhao Zhou and Jianfei Yang. HoloLLM: Multisensory foundation model for language-grounded human sensing and reasoning. In *The Thirty-ninth Annual Conference on Neural Information Processing Systems*, 2025. URL <https://openreview.net/forum?id=cHMP2IAhML>.
- [83] Haozhe Zhou, Riku Arakawa, Yuvraj Agarwal, and Mayank Goel. Imucoco: Enabling flexible on-body imu placement for human pose estimation and activity recognition. In *Proceedings of the 38th Annual ACM Symposium on User Interface Software and Technology*, UIST '25, New York, NY, USA, 2025. Association for Computing Machinery. ISBN 9798400720376. doi: 10.1145/3746059.3747695.

A Experiments and Implementation Details

A.1 Training Data and Window Construction

All AnyMo training stages use Nymeria [40] as the only source of motion-text supervision. We first synchronize Nymeria body motion, mesh vertices, atomic-action annotations, and real IMU streams to a common 60 Hz timeline. Most exported instruction-tuning rows correspond to 5 s windows: after removing IMU boundary tokens, 90.1% of rows contain 150 IMU code tokens, which corresponds to $T = 300$ frames because the original frame count is twice the IMU code-token count. The remaining text-aligned rows keep their native atomic-action durations, so T can be shorter or longer. Each frame contains six IMU channels (three-axis acceleration and three-axis angular velocity), and each window is represented on a fixed 23-node body graph following the Xsens kinematic tree: pelvis, spine, neck/head, both shoulders/arms/hands, and both legs/feet/toes. The graph representation has shape $6 \times T \times 23 \times 1$. For sparse wearable observations, only the nodes corresponding to the visible sensors are exposed to the model; the other graph nodes are replaced by the learned mask token in the encoder.

Before applying the held-out-subject protocol, the text-aligned Nymeria export contains 828 recording samples and 168,295 windows. We choose the held-out subjects so that the held-out split remains subject-disjoint while still covering all 20 original Nymeria scenarios. Specifically, we reserve five subjects (alec_meza, bradley_herman, dominique_frye, justin_ramirez, and kyle_parker), whose held-out recordings collectively cover the 20 scenarios, and exclude these recordings from the text-aligned token and instruction-tuning exports. The resulting subject-disjoint IMU-token pre-training corpus contains 808 Nymeria recording samples and 164,387 text-aligned windows. The instruction-tuning export contains 159,098 labeled windows and expands them into 986,322 language-model instruction rows, evenly split between narration and activity multiple-choice tasks. The same subject-disjoint export provides 986,322 paired IMU-text contrastive rows, using the original atomic-action narration and conservative augmented narrations as positive texts.

A.2 Synthetic IMU Generation

The synthetic pre-training signals are generated from Nymeria’s anatomically grounded human model, using its mesh and skeleton motion. For every body segment, we build a surface template from selected mesh vertices. At each candidate vertex, we estimate a local right-handed sensor frame from the surface normal, an anatomical tangent direction, and the corresponding binormal. The local offset between the posed mesh vertex and the segment coordinate frame is then tracked through the motion sequence, producing a dense set of geometry-aware candidate IMU placements. We define our surface selection from the template-mesh skinning weights. For each mesh vertex, we sort the influencing skeleton joints by skinning weight and assign the vertex to a body segment if one of that segment’s joints appears among the top two nonzero influences. This is a compromise between two less useful extremes: a strict top-1 assignment can make shared boundary vertices disappear from nearby segments, while treating every positive skinning weight as a candidate can spread each segment over overly broad and weakly related surface regions. The resulting selected vertex counts are shown in Table 5; in total, the exported synthetic archive contains 831 eligible Nymeria samples, each with 2,374 candidate placements across the 23 body segments.

Table 5: Selected surface vertices per body segment for synthetic IMU placement.

Segment	# Vertices	Segment	# Vertices	Segment	# Vertices
Pelvis	108	T8	105	Right Hand	145
L5	59	Neck	44	Left Shoulder	45
L3	35	Head	290	Left Upper Arm	90
T12	90	Right Shoulder	42	Left Forearm	120
Right Upper Arm	90	Left Hand	145	Left Upper Leg	106
Right Forearm	127	Right Upper Leg	108	Left Lower Leg	122
Right Lower Leg	122	Right Foot	125	Left Foot	112
Right Toe	72	Left Toe	72		

During representation pre-training, each training window is sampled twice to form two full-body graph views. For each segment in each view, one candidate placement is selected independently. We further apply surface rotation augmentation, with an in-plane rotation range of $\pm 180^\circ$ and a small tilt range of $\pm 10^\circ$ during training. Acceleration and angular velocity are computed from the simulated rigid-body trajectory in the candidate sensor frame. Real Nymeria IMU streams from the head and wrists are not used as training targets; they are used to estimate device-noise priors and to define the held-out sim-to-real evaluation protocol. We estimate this noise prior from the two Nymeria device streams and three real wearable sites to make the synthetic IMU signals more realistic.

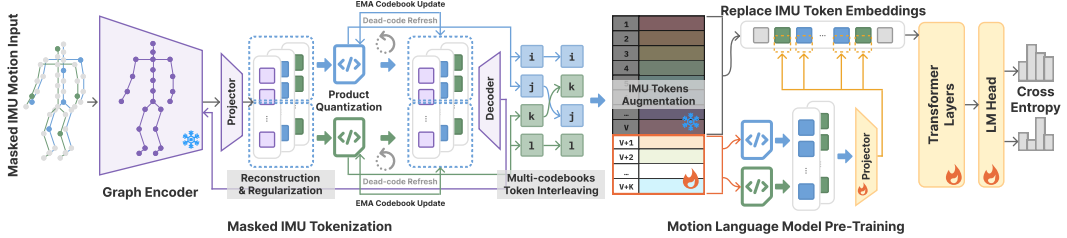


Figure 7: More details of Masked IMU Tokenization and Motion Language Model Pre-Training.

A.3 Representation Pre-Training and Tokenization

As illustrated in Figure 7, the IMU encoder is an ST-GCN [72] over the 23-node body graph. It uses ten spatio-temporal graph convolution blocks with temporal kernel size 9, channel widths increasing from 64 to 128 to 256, and two temporal stride-2 stages. Thus a 300-frame input window is encoded as a time-preserving latent sequence of length about 75, with latent dimension 256. Pre-training samples two independent full-body graph views from the synthetic candidate set and two corresponding sparse views. For each sparse view, a random number of visible nodes between 1 and 5 is retained, and all remaining nodes are masked. A six-layer Transformer [64] predictor maps the sparse-view latent sequence to the opposite full-view target sequence. We train with the symmetric predictive InfoNCE objective, temperature 0.1, and stop-gradient targets. Unless otherwise noted, the ST-GCN optimizer is AdamW with learning rate 3×10^{-4} , batch size 64, and 10 epochs. The ST-GCN encoder pre-training is run on a single NVIDIA L40S GPU.

Table 6: Final PQ-VAE tokenizer diagnostics for the exported IMU tokenizer. Perplexity and top- k code mass summarize codebook usage, while exact sequence collision is measured after interleaving the two codebook streams.

Metric	Codebook 0	Codebook 1
Used codes	2,033 / 2,048	2,046 / 2,048
Usage rate	99.27%	99.90%
Dead-code ratio	0.73%	0.10%
Perplexity	1,285.7	1,098.1
Top-1 code mass	1.46%	1.11%
Top-10 code mass	5.17%	4.96%
Exact sequence collision rate	0.61%	

After ST-GCN pre-training, we freeze the encoder and train a product-quantized VAE on masked sparse-view latent sequences. The tokenizer uses two codebooks with 2,048 entries each, a 128-dimensional bottleneck, and 64-dimensional code vectors per codebook. The product-quantizer codebooks are updated with exponential-moving-average (EMA) statistics using decay 0.99. To prevent unused IMU tokens from persisting, we apply dead-code refresh after each EMA update: within each codebook, entries whose accumulated usage falls below 20% of the average code usage are replaced by latent vectors sampled from the current mini-batch. The decoder reconstructs the frozen ST-GCN latent sequence with a SmoothL1 reconstruction loss plus the standard commitment loss. At export time, the two codebook indices are interleaved over time. Consequently, a 5 s Nymeria window normally yields 75 latent steps and 150 IMU code tokens, plus boundary tokens. We add 4,096 IMU code tokens and IMU boundary tokens to the LLM tokenizer, while keeping the

learned codebook vectors as the continuous representation behind those discrete token IDs. We report final tokenizer diagnostics in Table 6, including codebook usage, concentration statistics, and exact sequence collisions. These diagnostics check the tokenizer at two levels. At the codebook level, the near-complete usage rates and low dead-code ratios show that the product quantizer does not collapse to a small subset of entries. The perplexities, 1,285.7 and 1,098.1 out of 2,048 entries, indicate broad but non-uniform code usage, while the low top-1 and top-10 masses show that no small group of codes dominates the assignment distribution. At the sequence level, the exact sequence collision rate is computed after interleaving the two codebook streams over time; the 0.61% collision rate indicates that almost all tokenized IMU windows receive distinct discrete token sequences.

A.4 Motion-Language Training

AnyMo uses Qwen2.5-0.5B [51] as the language backbone. We implement the motion-language pre-training stage with ms-swift [81], using a custom AnyMo model registration that replaces IMU token embeddings with projected codebook vectors at runtime. All motion-language training stages are run on two NVIDIA L40S GPUs. The LLM is first adapted with an IMU-token language-modeling stage in which the assistant target consists of IMU token sequences exported from the frozen ST-GCN and tokenizer. The IMU code-token embeddings are not ordinary lookup rows: at runtime, each IMU token ID is mapped back to its product-quantizer code vector and projected into the Qwen hidden space by a two-layer MLP. The corresponding language-model head rows are initialized from the same projected code vectors. For this stage, we use full fine-tuning with bf16, a maximum sequence length of 1024, learning rate 10^{-4} , batch size 16, and 3 epochs.

Before instruction tuning, we augment the Nymeria atomic-action narrations with GPT-OSS-120B [48]. For each atomic-action text, we treat the original annotation as the ground-truth semantic anchor and generate five paraphrases that preserve the same action meaning while varying wording, conciseness, temporal emphasis, body-motion emphasis, and scene generality. We then run a GPT-OSS-120B self-verifier that checks whether the five variants preserve the atomic action, maintain the action order, avoid unobserved intent or invented content, and provide sufficient diversity. If the verifier rejects the whole set, we regenerate all five variants; if fewer than five variants fail, we repair only the rejected variants while keeping the accepted ones. The verifier is applied after each generation or repair step, with at most two additional regeneration/repair rounds, giving at most three verifier passes per atomic-action row.

For the label-contrastive branch, we construct a closed activity-label vocabulary from the same atomic-action annotations. We first ask GPT-OSS-120B to assign a free-form activity label to every atomic action. Because these free-form labels can differ substantially in surface form, we normalize them by lowercasing, removing punctuation and extra spaces, and canonicalizing leading articles such as “a”, “an”, and “the” before exact deduplication. We embed labels with Qwen3-Embedding-8B [79] and cluster labels with frequency at least five using a cosine-similarity threshold of 0.85. For clusters containing two or more labels, GPT-OSS-120B merges semantically close labels into either one simple label or a slash-separated label when multiple equivalent phrasings should be retained. Human experts review roughly 1,000 candidate labels, remove ambiguous categories, and finalize AnyMo-180, a 180-class activity-label vocabulary. The resulting AnyMo-180 label corpus turns Nymeria into one of the largest fine-grained IMU-based HAR training corpora, providing an activity vocabulary that goes beyond the small closed label spaces common in wearable HAR and helps mitigate coarse activity labels and fragmented activity vocabularies [20, 8, 6]. To label windows against AnyMo-180, we run GPT-5.4 nano twice as an enum-text classifier over the 180 classes. Rows with identical labels across the two runs are accepted directly. Disagreements are adjudicated by GPT-5.4 mini, and we retain only labels with a majority vote after adjudication. The two GPT-5.4 nano passes agree on 128,461 of 168,295 rows (76.33%); among the 39,834 disagreements, GPT-5.4 mini produces a majority label for 34,873 rows. After this filtering, 162,896 rows remain labeled, corresponding to 96.79% of the 168,295 candidate rows. We then perform a second class-wise audit over the curated label set to further improve label quality. For each candidate row, we use GPT-5.5 High to compare the assigned activity label against the current source-text annotation and the preceding and following source-text annotations to verify the local temporal context; inconsistent rows are relabeled or dropped under human-expert supervision. This final audit yields 158,138 labeled rows, corresponding to 93.96% of candidate rows. The class distribution is long-tailed, reflecting in-the-wild activity frequencies: per-class counts range from 18 to 19,696 rows, with a median of 342.5 and a mean of 878.54. The final label counts are reported in Table 7.

Table 7: AnyMo-180 activity-label vocabulary and counts.

Label	Count	Label	Count	Label	Count	Label	Count
walking / hiking	19,696	standing	7,411	sitting	5,906	play board games / cards / puzzle	5,873
placing items on a surface	4,758	picking up objects	4,248	slicing / chopping / cutting / dicing food	3,765	folding clothes / pants / towel / blanket	3,752
gesturing	3,716	dancing	3,254	kneeling	3,130	turning in place / turning / spinning	2,584
playing soccer / kicking ball	2,522	closing refrigerator / cabinet / drawer / closet / door	2,493	playing charades	2,476	playing badminton	2,419
eating	2,323	standing up and walking	2,239	walking while carrying objects	2,141	opening and closing refrigerator / cabinet / drawer / closet / door	2,116
using laptop	2,058	raising hand(s) / arm(s)	1,987	adjusting pillows / sofa pillows	1,979	pulling a drawer	1,941
side stepping exercise	1,887	opening refrigerator / cabinet / drawer / closet / door	1,828	yoga / stretching	1,778	placing items into a box / bag / container	1,584
watching tv	1,581	arranging decorations	1,536	closing refrigerator / cabinet / drawer / closet / door and walking	1,470	playing air hockey / playing table hockey / playing foosball	1,433
walking down stairs	1,345	walking up stairs	1,311	squatting	1,253	biking outdoors	1,165
writing	1,146	opening refrigerator / cabinet / drawer / closet / door and walking	1,114	throwing objects	1,036	lying	976
scooping food	971	making coffee	910	playing arcade game	882	drinking	872
drawing	857	marching in place	822	measuring appliance / furniture / door	802	stirring / mixing	795
hanging clothing	780	disposing trash	779	moving chair	703	spreading / unfolding blanket / clothes	664
twisting torso	635	scratching / touching face	623	adding food to container / pan	608	loading dishwasher / unloading dishwasher	601
adjusting blinds / adjusting curtains	593	rotating hands / arms	586	opening bag / package / pack / pouch	576	inspecting appliance / furniture	569
walking / stepping in place	555	cleaning tableware / kitchenware	549	stir-frying	544	lunges / lunging	541
playing table tennis	539	using phone	538	standing up	498	opening refrigerator / cabinet / drawer / closet and taking objects	477
adjusting stove / turning on stove / opening stove / turning stove knob	457	knee raises	447	sweeping	445	spreading sauce / cream / butter on bread / food	444
turning off / on light switch	441	turning on faucet	441	playing billiards	425	walking while picking up object	418
adjusting glasses	414	tiptoeing	412	opening a box / container	410	cleaning whiteboard	404
sitting down	398	poking food	393	folding / rolling / tearing / peeling tape	381	punching / shadowboxing	377
reading	374	seasoning food	367	walking with bike	353	running	352
turning / shaking / nodding head	346	looking under furniture	345	closing a box / container	340	jumping / hopping in place	319
looking around	319	playing catch	314	butt kicks	312	operating electric kettle	306
playing darts	302	stacking items	283	flipping food in pan	279	capping marker / bottle / jar	268
stationary biking / riding an exercise bike	267	opening bottle / jar	264	vacuuming / walking while vacuuming	256	washing hands	250
moving sofa / couch	249	cleaning a surface	243	jogging in place	243	standing foot rotation / ankle rotation	243
operating oven	240	pressing / mashing food in pan	240	pouring liquid	234	using microwave	224
peeling fruits / vegetable	223	moving table	221	alternating punches while stepping in place	218	foot tapping	217
inserting pillow into pillowcase	216	placing pan on stove	216	swinging on a swing	215	pulling blinds / pulling curtains	208
filling a container with liquid	195	organizing books / shelves	193	marching	187	front kicks	182
air writing	169	standing leg raise	168	drying hands	161	using washing machine	154
jogging	142	playing with rubik's cube	140	eating while playing board game	137	pouring food into container	137
plank / alternating plank	130	whisking / beating eggs	126	cracking egg	116	bicep curls	115
organizing kitchen items	114	stepper exercise / using stepper	114	moving bed	111	ab rollout exercise	110
organizing clothes / towels	110	untangling party decorations	110	kneading dough / shaping dough	109	adjusting clothing	108
making sandwich	89	seated leg raises	89	adjusting hair	85	catching objects	83
running in place	83	rolling a yoga ball	82	adjusting headset	80	playing with a pool noodle	80
mopping	77	using toaster	76	bowling	72	walking while drinking	72
checking smartwatch	69	opening trash bin	69	clapping	68	jumping rope	68
tearing paper towel / tearing tissue	68	pulling chair and sitting	65	wiping mouth with tissue / napkin / paper towel	61	removing seeds from food	59
tying shoe laces	57	walking while punching	51	playing toy	50	standing arm circles	47
washing fruit / vegetables	46	writing with foot	45	dumbbell lateral raises	43	setting up pool table	42
hanging decorations / frames	39	threading beads	38	standing elbow-to-knee crunch	35	sit-ups	34
sitting up	34	playing rock-paper-scissors	33	pruning flower	21	squeezing fruit	18

We then perform instruction tuning with both language-modeling and contrastive losses. The language-modeling branch contains two task families: IMU-to-narration generation and IMU-to-activity multiple choice. For each multiple-choice example, the correct activity is mixed with a fixed 35-choice candidate set sampled from the training activity pool. The contrastive branch encodes IMU prompts and text prompts with the same Qwen backbone, then applies branch-specific latent-attention poolers and projection heads before a symmetric IMU-text contrastive loss. The reported contrastive checkpoint uses an 8-token learnable soft prompt on the text/label branch. We train the contrastive instruction-tuning stage for 1 epoch with maximum sequence length 4096, learning rate 2×10^{-5} , contrastive temperature 0.05, language-modeling loss weight 1.0, and contrastive loss weight 2.0. For contrastive batches, we use a per-GPU batch size of 16 and 4 GradCache steps [15]; with NVIDIA L40S GPUs, this gives an effective global contrastive batch size of $16 \times 4 \times 2 = 128$.

A.5 Zero-Shot Recognition Evaluation

Downstream HAR datasets are used only for evaluation. All dataset adapters convert accelerometer channels to m/s^2 and gyroscope channels to rad/s when the source units are known, resample windows to 60 Hz, and map each physical device location to the closest node(s) in the 23-node body graph. For head-mounted video datasets such as Ego4D, EgoExo4D, and MMEA, the visible node is Head. For wrist, arm, waist, torso, leg, and foot sensors, the adapters expose the corresponding upper-limb, spine, or lower-limb graph nodes.

Each evaluation example is tokenized by the frozen ST-GCN and tokenizer, then scored without updating AnyMo. For recognition, we encode the IMU prompt and each candidate activity label prompt, compute cosine similarities in the learned contrastive space, and rank all labels from the dataset’s label vocabulary. Accuracy is computed from the top-ranked label, macro-F1 is computed over predicted labels, and Recall@2 is positive if the ground-truth label appears in the top two ranked labels. The label vocabulary is dataset-specific and includes all activities for that benchmark split, so the evaluation does not require dataset-specific classifier heads.

A.6 Retrieval and Captioning Evaluation

For sim-to-real evaluation on Nymeria, we export held-out examples from the five reserved subjects listed above. This produces 20 held-out recording samples and 3,908 text-aligned windows for both retrieval and captioning. For OOD evaluation on EgoExo4D, we construct a balanced 4,000-window atomic-action subset with 500 examples from each of eight parent tasks: rock climbing, basketball, dance, cooking, health, bike repair, soccer, and music. These windows are sampled from EgoExo4D’s 200 Hz head-IMU streams, resampled to 60 Hz, and tokenized with the same frozen AnyMo tokenizer.

Retrieval uses the same prompt templates as contrastive instruction tuning. For IMU-to-text retrieval, each IMU embedding is compared against the pool of primary reference narrations; for text-to-IMU retrieval, each text embedding is compared against the pool of IMU embeddings. We report Recall@1, Recall@5, Recall@10, and MRR in both directions. Captioning uses the IMU-to-narration prompt and greedy decoding with a maximum of 64 generated tokens. Generated captions are evaluated against the primary atomic-action narration using BLEU, ROUGE-L, METEOR, and BERT-F1. For BERT-F1, we compute it with the `deberta-xlarge-mnli` [22]².

A.7 Capability Radar Details

Figure 1 summarizes the main results with nine radar axes drawn from the three evaluation groups. Exact Activity Match, Balanced Recognition, and Top-2 Activity Recall correspond to the average zero-shot HAR Accuracy, macro-F1, and Recall@2 across the 14 downstream recognition datasets. IMU-to-Text Rank Quality and Text-to-IMU Rank Quality correspond to MRR for the two retrieval directions on the EgoExo4D zero-shot 100-sample candidate-ranking split. Word Match, Sequence Overlap, Content Alignment, and Semantic Similarity correspond to BLEU-1, ROUGE-L, METEOR, and BERTScore-F1 on the EgoExo4D zero-shot captioning split. Because these metrics have different natural ranges, the radar chart rescales each axis independently for visualization; the axis tick labels report the original metric values.

²<https://huggingface.co/microsoft/deberta-xlarge-mnli>

A.8 Ablation Implementation Details

All ablations in Table 4 use the same downstream zero-shot recognition protocol, candidate label vocabularies, and metrics as the full AnyMo model. When an ablation changes an upstream stage, all downstream artifacts that depend on that stage are regenerated, including the tokenizer export, IMU-token pre-training rows, instruction-tuning rows, and evaluation tokens. This keeps the comparison focused on the removed component rather than mixing incompatible tokenizers or encoders.

Geometry-aware simulation. The full model uses geometry-aware synthetic IMU generated from mesh-surface candidate placements, with local sensor frames estimated from surface normals and anatomical tangents as described in Section A.2. For *w/o geometry-aware simulation*, we instead generate synthetic IMU from a joint-mounted setup commonly used in prior synthetic-IMU work: one default virtual sensor is rigidly attached to each of the 23 Xsens segment frames. This removes mesh-vertex candidate placements, local surface frames, normal/tangent-based orientation variation, surface-rotation augmentation, and real-device calibration. All later stages are rerun from this synthetic data: the ST-GCN encoder is trained with the same masked cross-view predictive InfoNCE objective, the PQ-VAE tokenizer is retrained on the resulting sparse-view latents, the motion-language pre-training and instruction-tuning data are re-exported with that tokenizer, and the final AnyMo model is evaluated with the same recognition protocol. Because the joint-mounted setup provides only one placement per body node, it removes within-node device-placement diversity; this ablation tests whether conventional joint-level synthetic IMU is sufficient without dense geometry-aware setup variation.

Masked cross-view predictive contrastive pre-training. The full encoder objective samples two full-body graph views, samples sparse visible-node masks for each view, and trains a Transformer predictor to map each sparse-view latent sequence to the opposite full-view latent sequence with symmetric InfoNCE and stop-gradient targets. For *w/o masked cross-view pred. contrastive*, we keep the same synthetic graph-view sampling but replace this sparse-to-full predictive objective with a standard full-view contrastive objective. Concretely, the two independently sampled full graph views are encoded, projected, and contrasted directly against each other with sequence-level InfoNCE. No sparse visible-node mask and no sparse-to-full predictor are used in this encoder-pretraining ablation. The tokenizer, motion-language pre-training rows, instruction-tuning rows, and downstream evaluation tokens are then regenerated from this encoder.

Motion-language contrastive losses. The full contrastive instruction-tuning stage combines three losses: the language-modeling loss on instruction rows, a narration-level symmetric IMU-text contrastive loss between IMU prompts and atomic-action narration prompts, and a supervised label-level contrastive loss between IMU prompts and curated activity-label prompts. For *w/o label contrastive*, we set the label-level contrastive loss weight to zero while keeping the narration-level contrastive loss and the language-modeling loss unchanged. For *w/o narration contrastive*, we set the narration-level contrastive loss weight to zero while keeping the label-level contrastive loss and the language-modeling loss unchanged. For *w/o all contrastive*, we remove both contrastive branches and train only with the language-modeling instruction-tuning objective from the IMU-token pre-trained checkpoint.

MCQ instruction tuning. The full language-modeling branch is balanced between IMU-to-narration rows and IMU-to-activity multiple-choice rows. For *w/o MCQ instruction tuning*, we remove all MCQ instruction rows and replace them with additional narration rows, so that the total number of language-modeling instruction examples remains unchanged. The contrastive instruction-tuning losses and all other hyperparameters are unchanged for this ablation.

B AnyMo Bench

Beyond model training, AnyMo-180 also enables a controlled benchmark construction. We further derive **AnyMo Bench**, an in-the-wild HAR benchmark from real Nymeria IMU streams [40]. The benchmark is designed to stress two forms of generalization that are central to wearable sensing in realistic deployments: recognizing fine-grained daily activities on unseen subjects, and transferring across different IMU units mounted at the same body position. Such setup shifts are a persistent challenge for wearable HAR, where activity recognition can be affected by inter-subject motion variation, device hardware, exact body placement, orientation, and collection protocol [20, 8, 6]. Nymeria enables this evaluation because it contains synchronized real IMU streams from three

body positions: Head, Left Wrist, and Right Wrist with two co-located IMUs per position. In the cross-device setting, models train on the first IMU at each position and are tested on the second IMU at the same position, so the body placement is fixed while the IMU unit changes.

Evaluation settings. We use a subject-disjoint 8:2 split with seed 42, yielding 157 training subjects and 39 test subjects from 196 subjects. AnyMo Bench contains 154,695 activity windows and covers 211.6 hours of real in-the-wild IMU data. The split contains 123,874 training windows and 30,965 test windows for the eligible Fine150 label space, with no class missing from either split. We report four settings: *Fine150 / Unseen Subject*, *Fine150 / Unseen Subject + Cross Device*, *Core50 / Unseen Subject*, and *Core50 / Unseen Subject + Cross Device*. In the Unseen Subject settings, train and test examples use the first IMU at each body position. In the Unseen Subject + Cross Device settings, training uses the first IMU, but testing uses the second co-located IMU for the held-out subjects.

Label spaces. Fine150 is a fine-grained 150-class label space derived from AnyMo-180. Starting from the 180 curated classes, we remove labels that are unstable under the subject split, including classes with fewer than two test subjects or fewer than 10 test windows, and exclude a small number of highly context-dependent labels whose distinction depends heavily on visual or semantic context rather than IMU-observable motion. Fine150 remains long-tailed, with per-class counts ranging from 47 to 19,696 rows, a median of 411, and a mean of 1031.3. Core50 is a coarser 50-class label space (still more fine-grained than most existing IMU-based HAR datasets) built by merging Fine150 labels with IMU-pose-aware semantics: labels are combined when they share similar body-motion signatures, are low-sample, and remain interpretable as a coherent core activity. Large, motion-distinct, or already reliable classes are kept separate. After aggregation, Core50 class counts range from 72 to 19,696 rows, with a median of 1921 and a mean of 3093.9.

Table 8: IMU-based HAR baseline results on AnyMo Bench.

Model	Acc@1	Acc@5	Macro-F1
<i>Fine150 / Unseen Subject</i>			
DeepConvLSTM	35.3	63.0	<u>17.2</u>
MantisV2	38.5	65.2	22.8
COMODO	<u>37.8</u>	<u>65.2</u>	16.0
<i>Fine150 / Unseen Subject + Cross Device</i>			
DeepConvLSTM	1.9	9.5	0.4
MantisV2	<u>14.4</u>	<u>39.7</u>	8.6
COMODO	24.0	50.6	<u>8.0</u>
<i>Core50 / Unseen Subject</i>			
DeepConvLSTM	43.2	75.4	34.5
MantisV2	<u>45.8</u>	<u>76.8</u>	41.3
COMODO	46.2	78.8	<u>37.3</u>
<i>Core50 / Unseen Subject + Cross Device</i>			
DeepConvLSTM	1.8	12.1	0.6
MantisV2	<u>16.6</u>	<u>48.7</u>	<u>18.4</u>
COMODO	32.6	67.8	23.3

Baselines and metrics. We evaluate three baselines. DeepConvLSTM is a classic IMU-based HAR method [50], and MantisV2 is one of the best recent time-series classification foundation models [13]; both supervised IMU baselines are trained for 100 epochs on the AnyMo Bench training split. We also adapt COMODO, a self-supervised multimodal baseline for video-to-IMU representation learning [10], using MantisV2 as the IMU backbone and TimeSformer as the video backbone, and train it for 20 epochs. We synchronize all IMU streams to a common 60 Hz temporal grid to align the two co-located Nymeria IMU units at each body position, while preserving temporal detail that supports the fine-grained daily-activity taxonomy [58]. The resulting activity windows are variable length, with durations concentrated around 5 seconds. Across the eligible Fine150/Core50 windows, 129,331 of 154,695 windows (83.60%) contain 300 IMU timesteps, with lengths ranging from 60 to 1200 timesteps (1.0–20.0 s). For fixed-length baselines such as DeepConvLSTM, windows shorter than 300 timesteps are zero-padded and longer windows are split into non-overlapping 300-timestep segments, dropping any remaining tail. For baselines with model-specific variable-length handling,

such as MantisV2 and COMODO with a MantisV2 IMU backbone, IMU segments are resized to the model input length by interpolation. We report Acc@1, Acc@5, and macro-F1 to measure exact recognition, near-miss retrieval among many candidate activities, and class-balanced performance.

Results and implications. As shown in Table 8, the results indicate that AnyMo Bench is challenging. On Fine150 / Unseen Subject, MantisV2 and COMODO reach comparable top-line accuracy, with MantisV2 at 38.5% Acc@1 and 65.2% Acc@5 and COMODO at 37.8% Acc@1 and 65.2% Acc@5, while DeepConvLSTM reaches 35.3% Acc@1 and 63.0% Acc@5. These results are meaningful for a 150-class in-the-wild unseen-subject task, but the macro-F1 scores indicate substantial remaining difficulty on tail and fine-grained classes. Core50 improves recognition accuracy, with COMODO reaching 46.2% Acc@1 and 78.8% Acc@5, while MantisV2 obtains the strongest macro-F1 at 41.3%; however, the remaining error shows that reducing the label granularity does not make the task trivial. Cross-device evaluation remains much harder: COMODO gives the strongest cross-device Acc@1, reaching 24.0% on Fine150 and 32.6% on Core50, but the gap from same-device unseen-subject recognition remains large, revealing substantial room for same-position different-device transfer.

These results suggest that the difficulty comes not only from label granularity, but also from realistic subject and device shifts. Because the benchmark construction combines automatic label proposal, embedding-based semantic label consolidation, human-expert review, enum-label assignment, full class-wise auditing, relabel/drop decisions, and IMU-pose-aware label-space aggregation, AnyMo Bench provides a challenging, in-the-wild, and carefully curated testbed for future work on robust wearable motion recognition.

C Downstream Evaluation Dataset Details

The zero-shot recognition benchmark contains 14 downstream datasets that are never used for training AnyMo. Table 9 lists each dataset’s activity classes and sensor placements. Sensor placements are reported using readable AnyMo graph segment names exposed to the model during evaluation, after mapping each dataset sensor to the closest node(s) in AnyMo’s 23-node body graph. For EgoExo4D, Ego4D, and MMEA, we follow the train/test splits from COMODO [10]³. For OpenPack, we use the OpenPack Challenge 2022 split [74]⁴ and discard contiguous operation segments shorter than 1 s or longer than 30 s; this removes 204 of 10,512 valid labeled segments (1.94%) across the official split. For the remaining datasets, we use the train/test splits distributed with UniMTS [78]⁵.

Table 9: Downstream zero-shot HAR datasets, activity classes, and sensor placements.

Dataset	# Classes	Classes	Sensor Placements
Opportunity	4	stand, walk, sit, lie	L3, Right Upper Arm, Right Forearm, Left Upper Arm, Left Forearm
UCI-HAR	6	walk, walk upstairs, walk downstairs, sit, stand, lay	L5
w-HAR	7	walk, sit, stand, jump, lie down, stairs up, stairs down	Right Foot
RealWorld	8	lying, jumping, standing, walking, sitting, climbing down, climbing up, running	Left Shoulder, Left Forearm, Head, Left Foot, Left Upper Leg, Left Upper Arm, L5
TNDA-HAR	8	sitting, standing, lying down, ascending stairs, descending stairs, riding, walking, jogging	Right Forearm, Left Lower Leg, Right Hand, Left Foot, T8

³<https://github.com/cruiseresearchgroup/COMODO>

⁴<https://open-pack.github.io>

⁵<https://huggingface.co/xiyuanz/UniMTS>

Dataset	# Classes	Classes	Sensor Placements
EgoExo4D	8	Basketball, Bike Repair, Cooking, Dance, Health, Music, Rock Climbing, Soccer	Head
OpenPack	10	Picking, Relocate Item Label, Assemble Box, Insert Items, Close Box, Attach Box Label, Scan Label, Attach Shipping Label, Put on Back Table, Fill out Order	Right Forearm, Left Forearm, Right Upper Arm, Left Upper Arm
PAMAP2	12	lying, sitting, standing, walking, running, cycling, nordic walking, ascending stairs, descending stairs, vacuum cleaning, ironing, rope jumping	Right Hand, T8, Right Foot
USC-HAD	12	walk forward, walk left, walk right, walk upstairs, walk downstairs, run forward, jump up, sit, stand, sleep, elevator up, elevator down	Right Upper Leg
WISDM	18	walking, jogging, stairs, sitting, standing, typing, brushing teeth, eating soup, eating chips, eating pasta, drinking cup, eating sandwich, kicking ball, playing ball, dribbling ball, writing, clapping, folding clothes	Right Hand
DSADS	19	sitting, standing, lying on back, lying on right side, ascending stairs, descending stairs, standing in an elevator still, moving around in an elevator, walking slowly, walking on a treadmill in flat positions, walking on a treadmill in inclined positions, running on a treadmill fast, exercising on a stepper, exercising on a cross trainer, cycling on an exercise bike in horizontal positions, cycling on an exercise bike in vertical positions, rowing, jumping, playing basketball	T8, Right Hand, Left Hand, Right Lower Leg, Left Lower Leg
UTD-MHAD	27	right arm swipe to the left, right arm swipe to the right, right hand wave, two hand front clap, right arm throw, cross arms in the chest, basketball shoot, right hand draw x, right hand draw circle (clockwise), right hand draw circle (counter clockwise), draw triangle, bowling (right hand), front boxing, baseball swing from right, tennis right hand forehand swing, arm curl (two arms), tennis serve, two hand push, right hand knock on door, right hand catch an object, right hand pick up and throw, jogging in place, walking in place, sit to stand, stand to sit, forward lunge (left foot forward), squat (two arms stretch out)	Right Hand for labels 0–20; Right Upper Leg for labels 21–26

Dataset	# Classes	Classes	Sensor Placements
Ego4D	31	baker, bike, bike mechanic, biology experiments, car / commuting / road trip, car / scooter washing, carpenter, cleaning / laundry, cooking, crafting / knitting / sewing / drawing / painting, cycling / jogging, eating, farmer, fixing something in the home, gardening, household management / caring for kids, indoor navigation (walking), construction / renovation jobs, playing board games, playing cards, playing games / video games, playing with pets, potting plants (indoor), practicing a musical instrument, reading books, scooter mechanic, walking on street, watching tv, working at desk, working out at home, working out outside	Head
MMEA	32	upstairs, downstairs, drinking, fall, reading, sweep floor, cut fruits, mop floor, writing, wipe table, wash hand, standing, play phone, type pc, eating, cooking, pick up phone, drop trash, fold clothes, walking, play card, brush teeth, wash dish, moving sth, type phone, chat, open close door, ride bike, sit stand, take drop sth, shopping, watch TV	Head

D Baseline Details

All baselines are evaluated with the same dataset-specific candidate activity vocabularies used by AnyMo. For ImageBind [16] and IMU2CLIP [44], we use the checkpoints pre-trained on Ego4D for all non-Ego4D recognition datasets. For Ego4D evaluation, we instead pre-train each baseline on MMEA and evaluate the resulting checkpoint on Ego4D, avoiding an Ego4D-pre-trained checkpoint on the Ego4D target dataset. Both ImageBind and IMU2CLIP use the same 60 Hz temporal setting as AnyMo. For IMUGPT [32], we follow the released default configuration and use its 20 Hz IMU input setting. For HARGPT [27], we follow the default prompt-based setting and feed IMU at 10 Hz. For UniMTS [78], we use the released checkpoint generated and pre-trained at 20 Hz, and evaluate it under the same 20 Hz setting. For NormWear [39], we follow the official implementation and its 65 Hz input setting. For the Gemma 4 26B text and plot baselines [17], we downsample IMU inputs to 10 Hz; even at 10 Hz, we use a 65,536-token context window so that all benchmark datasets can be processed without truncation.

E Prompt Analysis

E.1 Prompt Sensitivity

Zero-shot recognition embeds each candidate activity label through the language backbone, so the text-side representation is sensitive to how the label is prompted. To quantify this effect, we evaluate four fixed prompt formats with the same recognition protocol as Table 1. The fixed prompts are: *bare label*, which uses the class name directly; *person prompt*, “a person is {label}”; *IMU prompt*, “wearable IMU motion of {label}”; and *activity prompt*, “the activity is {label}”. We compare them with the final AnyMo setting, which replaces manual text templates with an 8-token learnable soft prompt on the text/label branch.

The fixed prompts produce noticeably different rankings even though the label vocabulary, IMU embeddings, and evaluation protocol are unchanged. For example, the IMU-centric template is weaker than the person- and activity-centric templates on this benchmark, indicating that manually written label contexts can shift the text embeddings in ways that are not consistently beneficial for recognition. The learnable soft prompt avoids committing to a hand-written template: during

Table 10: Prompt sensitivity for zero-shot HAR. Results averaged over 14 downstream datasets.

Text-side prompt	Acc	F1	R@2
Bare label	33.1	25.9	54.3
Person prompt	35.1	28.4	54.8
IMU prompt	28.3	22.5	47.0
Activity prompt	35.2	28.0	56.1
Learnable prompt (AnyMo)	35.7	29.5	57.5

contrastive instruction tuning, it learns a task-specific textual context for activity labels that better matches the IMU embedding space. This also removes the need to choose a dataset-specific prompt template at evaluation time. Accordingly, AnyMo uses the learnable prompt in all final zero-shot recognition results, where it gives the best average Acc, F1, and Recall@2 among the compared single-prompt settings.

E.2 Prompt Templates

Figure 8 summarizes the text templates used by AnyMo. The IMU-token language-model pre-training stage is trained to generate IMU token sequences. The narration and MCQ instruction templates are used during language-modeling instruction tuning; captioning evaluation uses the narration template, and MCQ-style evaluation uses the MCQ template. The contrastive IMU and text templates are used during contrastive instruction tuning and are used for retrieval and zero-shot recognition, with the learnable soft prompt prepended to the text/label branch in the final AnyMo checkpoint.

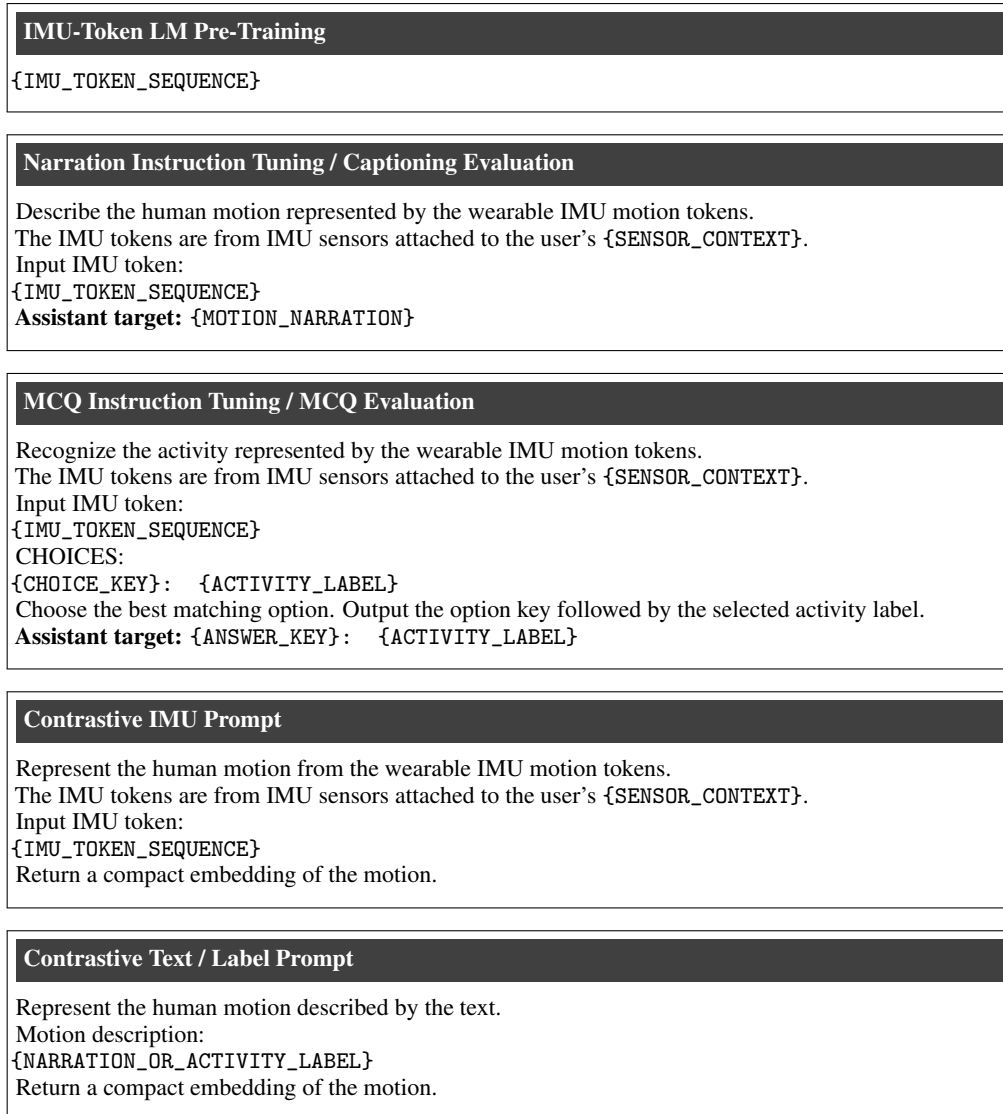


Figure 8: Prompt templates used for motion-language pre-training, instruction tuning, contrastive tuning, and evaluation.